The Diurnal Cycle of Tropical Cloudiness and Rainfall Associated with the Madden–Julian Oscillation

NAOKO SAKAEDA AND GEORGE KILADIS

NOAA/Earth System Research Laboratory, Physical Sciences Division, Boulder, Colorado

JULIANA DIAS

Cooperative Institute for Research in Environmental Sciences, University of Colorado, and NOAA/Earth System Research Laboratory, Boulder, Colorado

(Manuscript received 1 November 2016, in final form 13 January 2017)

ABSTRACT

This study examines the diurnal cycle of rainfall and cloudiness associated with the Madden–Julian oscillation (MJO) using TRMM rainfall rate and ISCCP multilevel cloud fraction data. There are statistically significant differences in diurnal cycle amplitude and phase between suppressed and enhanced envelopes of MJO convection. The amplitude of the diurnal rainfall rate and middle–deep cloudiness increases within enhanced MJO convection, especially over the ocean. However, the differences in diurnal cycle amplitude between enhanced and suppressed MJO are generally smaller than the differences in daily mean values, so that its relative contribution to total rainfall or cloudiness variance within enhanced MJO convection becomes smaller. Near the coastlines of islands within the Maritime Continent, the diurnal cycle amplitude tends to increase 5–10 days prior to the arrival of the peak enhanced MJO convection, but this relationship is weaker over the interior areas of larger islands where the climatological diurnal amplitude is already large. Within enhanced MJO convection, the diurnal rainfall peak is frequently delayed by about 3 h and cloud height decays at slower rate compared to suppressed conditions. More stratiform rainfall occurs following the peak convective rainfall within enhanced MJO convection, delaying the total rainfall peak by a few hours as a result of its greater horizontal extent. The results of this study suggest that the MJO modulates both the amplitude and phase of the diurnal cycle of tropical rainfall and cloudiness by influencing cloud type population distribution and associated rainfall rates.

1. Introduction

The Madden–Julian oscillation (MJO; Madden and Julian 1971, 1972) is a multiscale phenomenon, consisting of a hierarchy of cloud systems from synoptic scale to individual cumulus clouds within its planetary envelope of organized convection (e.g., Nakazawa 1988; Hendon and Liebmann 1994; Dias et al. 2013, 2017). In this study, we focus on the relationship between the MJO and the diurnal cycle of rainfall and cloudiness.

The diurnal cycle and other embedded sub-MJO-scale phenomena such as mesoscale convective systems and convectively coupled equatorial waves are generally enhanced within the envelope of enhanced MJO convection (Chen and Houze 1997; Straub and Kiladis 2003; Yasunaga and Mapes 2012; Dias et al. 2013, 2017). Some studies suggest that these subscale features are the drivers of the MJO, transferring heat, momentum, and moisture upscale to generate the planetary features of the MJO (e.g., Biello and Majda 2005; Majda and Stechmann 2009; Maloney 2009) or forming a planetary-scale wave packet (Yang and Ingersoll 2011, 2013). If these features are indeed important to MJO dynamics, then some systematic relationships may be expected between MJO characteristics and the embedded subscale phenomena. However, the manner in which these phenomena vary with the MJO is not well documented. To better understand the potential significance of the subscale phenomena to the MJO, this study specifically focuses on the diurnal cycle to supplement the recent work of Dias et al. (2017) and Kikuchi et al. (2017), who examine synoptic and mesoscale organization embedded within the MJO.

As one of the fundamental modes of atmospheric variability, the diurnal cycle explains a large portion of the variance of tropical cloudiness and rainfall (Yang

Corresponding author e-mail: Naoko Sakaeda, naoko.sakaeda@noaa.gov

DOI: 10.1175/JCLI-D-16-0788.1

and Slingo 2001; Kikuchi and Wang 2008). Theoretical and observational studies suggest that the diurnal cycle of rainfall and cloudiness can be important for preconditioning the convective onset or propagation of the MJO and other equatorial waves (Johnson et al. 1999; Raupp and Silva Dias 2009; Peatman et al. 2014; Ruppert and Johnson 2015; Majda and Yang 2016). Better representation of the diurnal cycle and its interaction with the MJO also appears to improve simulation skill of the MJO and seasonality in some general circulation models (Neale and Slingo 2003; Bernie et al. 2008). Peatman et al. (2014, 2015) suggest that the accurate representation of the interaction between the MJO and diurnal cycle is key to realistic simulation of propagation and spatial and temporal scales of the MJO, especially over the Maritime Continent (MC). Previous studies have shown that the diurnal cycle can vary with the MJO and other equatorial waves, yet a majority of those studies are limited in region or in their sample size of MJO events (e.g., Chen and Houze 1997; Sui et al. 1997; Rauniyar and Walsh 2011; Oh et al. 2012; Fujita et al. 2011; Vincent et al. 2016). For example, Sui and Lau (1992) and Oh et al. (2012) found that the amplitude of the diurnal rainfall cycle over the islands of the MC is weaker when MJO enhanced convection is present. Over the ocean, Sui et al. (1997), Tian et al. (2006), Fujita et al. (2011), and Rauniyar and Walsh (2011) found that the diurnal cycle amplitude of rainfall and deep convection is enhanced within MJO enhanced convection, suggesting that the influence of the MJO on the diurnal cycle amplitude differs between land and ocean. In addition, there are varying results from previous studies on how the MJO may impact the diurnal phase of rainfall and cloudiness. For example, Chen and Houze (1997), Fujita et al. (2011), Oh et al. (2012), and Rauniyar and Walsh (2011) found an MJO influence on the diurnal phase, but Tian et al. (2006) and Suzuki (2009) suggest that there is no such relationship.

There is a long history of research on the diurnal cycle of rainfall and cloudiness in the tropics, beginning with surface-based observations over land, ships, and small islands (e.g., Kraus 1963; Gray and Jacobson 1977; Dorman and Bourke 1979; Kousky 1980). The advent of satellite products enabled the examination of the diurnal cycle from a global perspective over the open ocean. A number of studies used satellite longwave irradiance (Hartmann and Recker 1986, Augustine 1984; Albright et al. 1985; Hendon and Woodberry 1993; Janowiak et al. 1994; Cairns 1995; Yang and Slingo 2001) and the Tropical Rainfall Measuring Mission (TRMM) satellite Precipitation Radar and microwave imagery (e.g., Nesbitt and Zipser 2003; Kikuchi and Wang 2008; Yang and Smith 2008) to examine the global diurnal cycle over the tropical ocean. In general, these past studies showed clear differences in the diurnal cycle over land versus ocean. Over land, the primary peak in rainfall tends to occur in the afternoon, driven by thermal destabilization of the atmosphere from solar radiative heating of Earth's surface during daytime (Yang and Smith 2006). Over the ocean, the diurnal amplitude is relatively weak compared to land, but rainfall tends to peak between midnight and early morning.

Several differing theories have been proposed to explain the nocturnal peak of the rainfall over open water. One speculates that nocturnal radiative cooling at cloud tops destabilizes the upper troposphere and raises the height of the tropopause, thus encouraging high clouds and rainfall to peak at night time (Kraus 1963; Randall et al. 1991). A second mechanism relies on the difference in the radiative heating between cloudy and clear-sky regions. At night, there would be relatively more radiative cooling within clear than cloudy regions, resulting in low-level convergence into cloudy regions, helping to further organize convection (Gray and Jacobson 1977). Yet another mechanism also considers interactions between convection and the ocean surface to be important. Large diurnal variability of sea surface temperature (SST) has been observed, especially during days with clear skies and calm winds (Matthews et al. 2014; Ruppert and Johnson 2015). Following the diurnal peak of tropical SST in the afternoon, clouds are observed to form and some of those continue to grow and mature at night (Chen and Houze 1997). Other studies suggest an effect of the semidiurnal tides on the early morning rainfall over water (Deser and Smith 1998; Dai 2001). Near the coasts, diurnal propagation of rainfall between land and ocean tends to occur through gravity waves and land–sea breezes (Dai 2001; Yang and Slingo 2001; Mapes et al. 2003; Kikuchi and Wang 2008; Tulich and Kiladis 2012; Biasutti et al. 2012).

Despite its prominence, no consensus has been reached on the mechanisms responsible for the diurnal cycle, especially over the open tropical ocean. This is likely because the diurnal cycle of rainfall and cloudiness results from complicated interactions among radiation, moisture, clouds, and surface characteristics that are yet to be accurately modeled. These local interactions can be altered by large-scale environmental variability associated with intraseasonal, interannual, and seasonally varying states. This study attempts to understand how the diurnal characteristics of cloud types and rainfall vary with respect to the MJO through the use of multiple global satellite datasets. In addition to the amplitude and phase of diurnal cycle, which have been examined previously, this study provides a more

detailed analysis of how the diurnal distribution of rainfall rate and cloud height varies between enhanced and suppressed phases of the MJO. We anticipate that these diagnostics will also prove useful for evaluating the skill of models in representing the relationship between the MJO and the diurnal cycle.

2. Data and methodology

a. Analysis of rainfall and cloudiness diurnal cycle

The diurnal cycle of rainfall is examined using the TRMM 3B42 version 7 product with 3-hourly and 0.25° horizontal resolution (Huffman et al. 2007). TRMM 3B42 products combine microwave data from multiple satellites including the TRMM Microwave Imager (TMI; 2A12; Kummerow et al. 2001), Precipitation Radar (PR; 2A25; Iguchi et al. 2000), satellite infrared (IR), and rain gauge data to generate high spatial and temporal coverage. This study also uses TRMM 3G68 version 7 PR data, which contain hourly rainfall rate estimates at 0.5° horizontal resolution (this data are available through the NASA precipitation processing system https://pps.gsfc.nasa.gov). The temporal and spatial coverage of TRMM 3G68 PR is more sparse than the 3B42 product, yet it allows us to better examine rainfall characteristics such as convective versus nonconvective rainfall. To maintain a consistent resolution between TRMM 3B42 and 3G68 data, the 3B42 rainfall rate data are regridded from its original 0.25° to 0.5° horizontal resolution, and the temporal resolution of TRMM 3G68 data is reduced by averaging on bins centered at the same 3-hourly span (in UTC) as 3B42 data.

The diurnal cycle of cloudiness is examined using 3-hourly and 2.5° horizontal resolution IR cloud fraction by cloud-top pressure from the International Satellite Cloud Climatology Project (ISCCP) D1 cloud product (Rossow and Schiffer 1999). The horizontal resolution of the cloud fraction data is coarser than the TRMM data, but ISCCP allows us to examine the diurnal evolution of cloud type and height. Some previous studies used higher-resolution brightness temperature to examine the diurnal cycle of cloudiness (e.g., Albright et al. 1985; Hendon and Woodberry 1993; Chen and Houze 1997; Yang and Slingo 2001; Suzuki 2009). In those studies, threshold values are often used to separate the diurnal cycle by cold and warm clouds and also to eliminate the diurnal cycle from clear-sky surface temperature. Thresholding can be useful for separating clouds according to their cloud-top temperature, but it is not suitable for examining the variability of diurnal cycle with the MJO, since a large number of days would be removed under suppressed MJO conditions. It is also difficult to objectively separate the diurnal cycle of clouds from clear-sky surface temperature fluctuations. For these reasons, we instead use the ISCCP cloud fraction data, which estimate the cloud-top pressure by using retrieved cloud-top temperature and atmospheric temperature profiles with pressure, eliminating the use of subjective threshold values.

We focus on the overlapping years of TRMM and ISCCP data, 1998 through 2009, to examine the diurnal cycle associated with a consistent set of MJO events. This study examines November through March (NDJFM) because this is the period when the MJO is climatologically most active (Roundy and Frank 2004; Zhang and Dong 2004). The diurnal amplitude and phase are estimated through harmonic analysis (e.g., Hartmann and Recker 1986; Yang and Slingo 2001). Days with any missing 3-hourly data are excluded. The same harmonic analysis is not applied to TRMM 3B68 PR data, which does not have enough samples to resolve the diurnal cycle at each grid point. Negri et al. (2002) suggested combining TRMM PR data over 12° wide or greater areas in order to adequately capture the diurnal cycle. Using this approach, the diurnal probability distribution of rainfall rates over selected geographical domains is used to compare TRMM 3G68 PR and 3B42 data in this study. Throughout the paper, the amplitude of diurnal cycle refers to that of the first diurnal harmonic. We have repeated the analysis using the diurnal range (i.e., difference between maximum and minimum value within a day) as the amplitude of diurnal cycle, and the general qualitative conclusions remain the same.

NOAA/NESDIS ETOPO1 topography data (Amante and Eakins 2009) are used to classify land and ocean grid points. The percentage of ETOPO1 grid points with an altitude greater than 0 within each grid cell of TRMM and ISCCP is used to calculate the fractional coverage of land in each grid cell. In the present study, any grid cell with greater than 10% land coverage is categorized as land. The same analysis is repeated with the percentage land coverage threshold as 100%, in order to test the sensitivity of results to the inclusion of coastal land. The sensitivity to this threshold value is discussed throughout the paper.

TRMM 3B42 data have known issues in capturing rainfall over high topography (Dai et al. 2007; Romilly and Gebremichael 2011; Matthews et al. 2013), so this study focuses on the general impact of the MJO over all land and ocean regions, separately, within the Indo-Pacific basin rather than focusing on any particular region. The temporal resolution of the datasets also limits us to only obtaining estimates of the timing of the diurnal cycle to within 3-h increments. The statistical significance of all results is tested using a 1000-member bootstrap

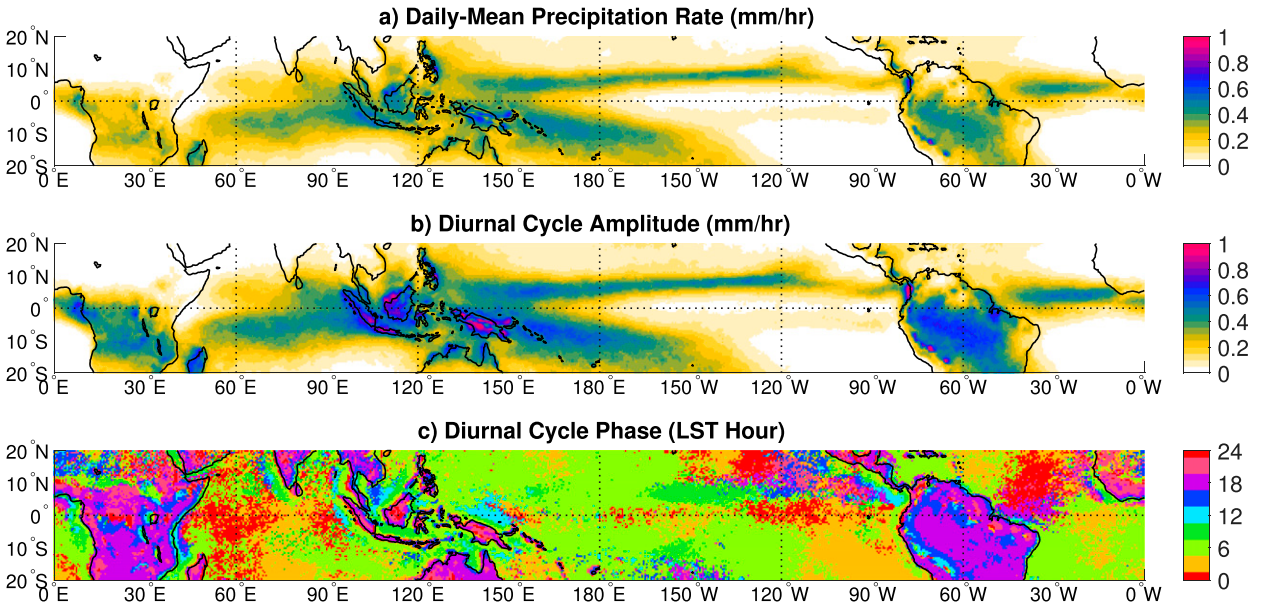

FIG. 1. NDJFM climatology of TRMM 3B42 rainfall rate (a) daily mean (mm h^{-1}), (b) diurnal amplitude (mm h^{-1}), and (c) diurnal phase (LST hour of day).

resampling test at the 95% confidence level. The error intervals throughout the manuscript are based on the 5th and 95th percentile of the bootstrapped samples.

b. *MJO identification*

Daily 2.5° horizontal resolution NOAA interpolated outgoing longwave radiation (OLR; Liebmann and Smith 1996) is used to isolate the MJO signal. The annual cycle and its first three harmonics are first removed, and anomalies are filtered using the MJO space–time frequency band (30–96-day periods and eastward wavenumbers 1–9 plus wavenumber 0; Wheeler and Kiladis 1999). Enhanced MJO convection is determined to be present at a grid point when the MJO-filtered OLR anomaly is below the lower 15th percentile of its NDJFM values between 15°N and 15°S during the study period, and the upper 15th percentile is used to identify MJO suppressed convection. The 15th percentile values are about $\pm 8\,W\,m^{-2}$, which is close to one standard deviation of the MJO-filtered anomaly at the edges of active MJO convective basins (e.g., Indo-Pacific basin) during NDJFM (see Fig. 1 of Kiladis et al. 2005). When combining the MJO-filtered OLR anomaly with higher horizontal resolution TRMM, the presence of the MJO is determined by the value of the OLR anomaly in the grid box that contains the higher-resolution point. This MJO-filtered OLR is used rather than other commonly used indices such as the real-time multivariable MJO index (RMM; Wheeler and Hendon 2004), since those indices are not as suitable for determining local convective activity of the MJO (Straub 2013; Kiladis et al. 2014).

3. Results

a. *November–March climatology*

Figure 1 shows the NDJFM mean of daily mean value, amplitude, and phase of the diurnal cycle from TRMM 3B42 rainfall rate. Yang and Slingo (2001) calculated the mean phase of the diurnal cycle by first finding the mean diurnal time series of rainfall rate and then finding the phase, but this method can lead to misrepresentation of the mean phase in cases where the diurnal phase has a bimodal distribution (Yang and Smith 2006; Nitta and Sekine 1994). For example, while most rainfall peaks at around 0300 local solar time (LST), less frequent but strong peaks around 1800 LST can cause the mean diurnal time series to peak erroneously at around 1800 LST. To avoid this problem, the diurnal phase is first estimated for each day in LST. The mean of the daily diurnal phase is calculated after shifting the phase to be centered around its mode during NDJFM at each grid point, then shifting the mean back to the original quantity.

Consistent with previous studies, the diurnal amplitude (Fig. 1b) broadly follows the mean values (Fig. 1a) and is greater over land than ocean, while coastal regions tend to have a amplitude similar to that of adjacent land. The diurnal amplitude tends to exceed the daily mean value over land, as was also found by Peatman

et al. (2014) over the MC (Figs. 1a,b). There is a clear contrast in the phase of the diurnal cycle between land and ocean (Fig. 1c), peaking between the late afternoon and evening over land and between midnight and morning over the ocean (e.g., Yang and Slingo 2001; Nesbitt and Zipser 2003; Kikuchi and Wang 2008). The gradients in the diurnal cycle phase near coastal areas reflect the diurnal propagation of rain (Dai 2001; Mapes et al. 2003; Mori et al. 2004; Sakurai et al. 2005; Biasutti et al. 2012).

A few studies have found that the general amplitude and phase of the diurnal cycle agree between the TRMM 3B42 and 3G68 PR data, except that the diurnal peak in the TRMM 3B42 data tends to lag that in the TRMM PR data by 3 h (Yang and Smith 2006; Yamamoto et al. 2008; Kikuchi and Wang 2008). We also found similar phase lags between these datasets as will be further discussed in section 3b(2).

Cloud fraction from ISCCP is separated by cloud-top pressure P_c as low cloud ($680 < P_c \leq 1000$ hPa), middle cloud ($440 < P_c \leq 680$ hPa), high cloud ($180 < P_c \leq 440$ hPa), and deep cloud ($P_c \leq 180$ hPa). Deep cloud is often combined with high cloud in previous studies (Cairns 1995; Myers and Waliser 2003); however, they are separated here because we find that they have a different diurnal phasing. The term ''deep cloud'' is adopted, but clouds at those altitudes are not necessary vertically thick, as for example would be the case for cirrus clouds. However, the deep cloud fraction defined here is highly correlated with rainfall rate, suggesting that it is mostly dominated by precipitating, vertically thick clouds.

Figure 2 shows the NDJFM mean of daily mean cloud fraction for each cloud type (Figs. 2a–d) and for total cloud (Fig. 2e). The fraction of low cloud is generally higher over ocean than land, especially over the eastern Pacific and eastern Atlantic basins, and subtropical latitudes where the total cloud fraction and rainfall rate (Fig. 1a) are low but where marine stratus decks prevail. In contrast to low cloud fraction, middle and high cloud fraction tend to be higher over land than ocean.

The geographical patterns in the diurnal amplitude of cloud fraction are generally similar to the patterns of their daily mean value for each cloud type fraction (Fig. 3). The diurnal cycle amplitude of low cloud is higher over the ocean, whereas the opposite is true for middle, high, and deep cloud fraction. It is notable that the amplitude of the diurnal cycle of total cloud fraction over the ocean is highest over the regions of marine stratus (Fig. 3e) because of the large amplitude of the low cloud fraction amount, whereas in regions of high rainfall rate over the warm pool there is weaker diurnal variability. Figure 4 shows that this is because the phase of the diurnal cycle differs vastly with cloud type. Low cloud fraction tends to peak in the early afternoon over land, whereas it tends to peak between midnight and late morning over the ocean (Fig. 4a). Middle cloud fraction tends to peak 3–9 h earlier than low cloud fraction over both land and ocean. The peak of middle cloud fraction generally follows that of high cloud fraction, which tends to peak between the afternoon and midnight over ocean and around midnight over land (Fig. 4c). These phasings agree with the results of Cairns (1995); however, Cairns (1995) did not show the difference in the diurnal cycle phase between high and deep cloud fraction, which were combined in his study. The deep cloud fraction tends to peak in the early morning hours over the ocean and from the late afternoon to early evening hours over land, and its peak leads that of high clouds by 3–6 h over land and by 3–9 h over the ocean, depending on the basin considered. The diurnal cycle of deep clouds is closest to being in phase with that of rainfall rate (Fig. 1c), which is likely a result of the highest rainfall rates being associated with deep cloud fraction even though this type is the least frequent when compared with the others (Fig. 2).

To summarize, the climatological diurnal phase of total cloud fraction represents the diurnal phase of cloud types that are most abundant at each region, which in turn display large contrasts between land and ocean. Rainfall rate and deep cloud fraction tend to peak during the afternoon over land and from around midnight to the early morning hours over the ocean.

b. *Variability associated with the MJO*

1) AMPLITUDE OF DIURNAL CYCLE

The relationship between the amplitude of the TRMM 3B42 diurnal cycle and MJO-filtered OLR is first examined through point-by-point cross-spectral analysis. For the cross-spectral analysis, missing dates are filled with a climatological value of that day of year in order to generate a continuous time series. The coherence and phase between daily time series of MJO-filtered OLR anomalies and the amplitude of the diurnal cycle of TRMM 3B42 rainfall rate are calculated using a 193-day window centered on every 15 January. Each window is tapered by a squared cosine function and Fourier coefficients are averaged over intraseasonal frequencies (i.e., between 30 and 96 days) before the coherence and phase are calculated. The distribution of this coherence is generated by bootstrap sampling the centered days of moving windows within January 1000 times, and this distribution is compared with a distribution of noise to test the statistical significance. Following the method of Kiladis et al. (2016), the noise distribution is calculated by applying the same cross-spectral analysis and bootstrap sampling to one of the time series reversed in time to preserve its temporal autocorrelation.

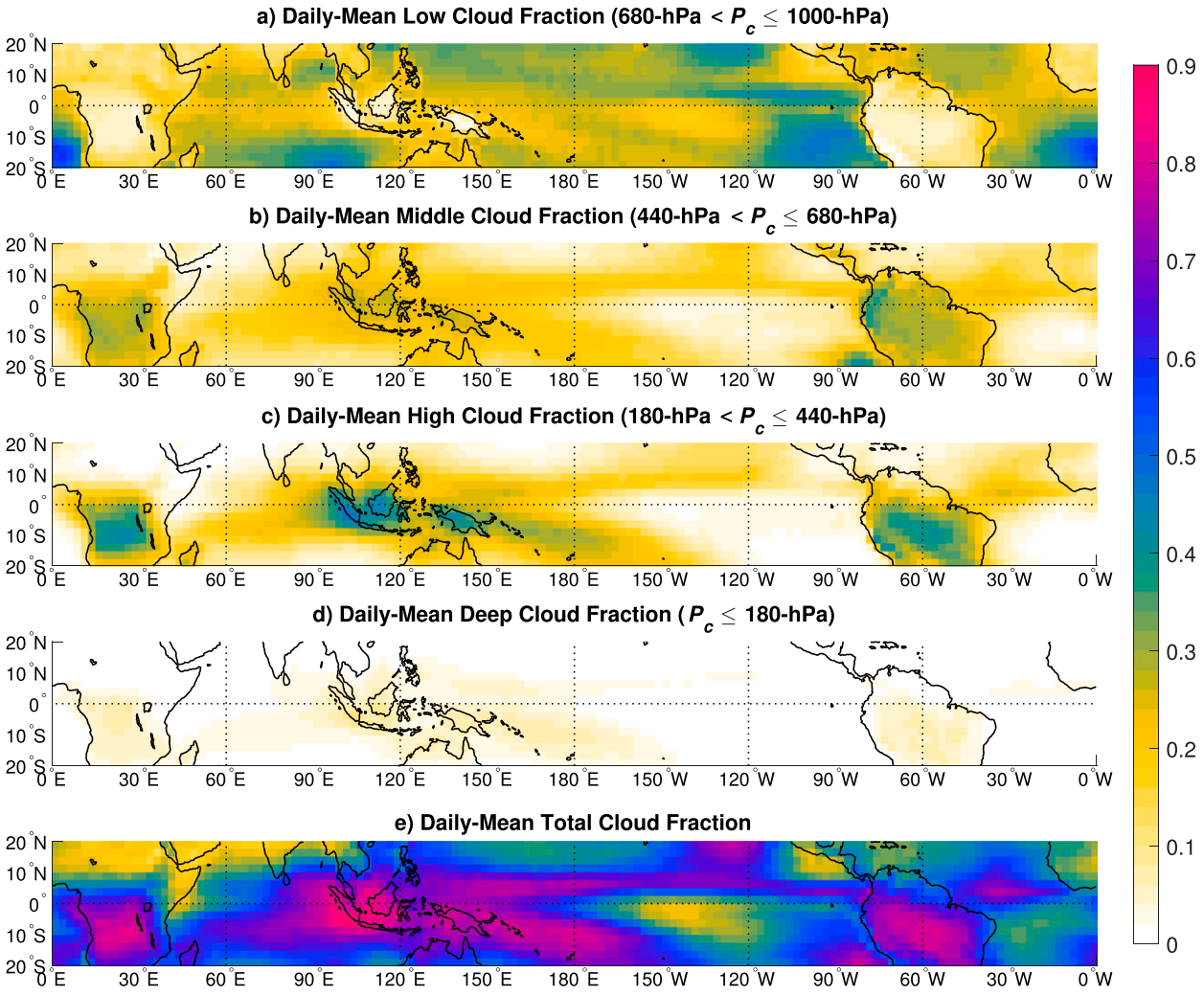

FIG. 2. NDJFM climatology of daily mean cloud fraction. (a) Low cloud fraction with $680 < P_c \leq 1000$ hPa; (b) middle cloud fraction with $440 < P_c \leq 680$ hPa; (c) high cloud fraction with $180 < P_c \leq 440$ hPa; (d) deep cloud fraction with $P_c \leq 180$ hPa; and (e) total cloud fraction [sum of (a)–(d)].

Figure 5 shows the coherence squared and phase between the daily MJO-filtered OLR anomaly and daily amplitude of the diurnal cycle of TRMM 3B42 rainfall rate. Figure 5c shows the confidence level where the coherence squared is statistically significantly different from noise. Rather than masking the region that is under a significance threshold level, we show the significance level separately to reveal how sharply the coherence varies geographically. The phase is plotted with respect to the negative extremes in MJO-filtered OLR (i.e., enhanced MJO), with a positive phase indicating that the peak in the amplitude of diurnal cycle lags the negative peak in MJO-filtered OLR anomaly. The average MJO period is 40–50 days, so a 90° phase indicates a lag of around 10–13 days.

Significant coherence between the MJO-filtered OLR anomaly and the amplitude of the diurnal cycle of rainfall rate appears mostly over the oceanic regions of the Indian Ocean through western Pacific basins (Fig. 5a) with a generally slight negative phase lag (Fig. 5b). This means that the amplitude of the diurnal cycle of rainfall peaks within the convectively enhanced envelope of the MJO, yet the peak in the amplitude of the diurnal cycle tends to lead the peak in the intensity of MJO enhanced convection by 1–3 days. The phase lag becomes greater near the coastlines of the MC, where the negative 30°–90° phase indicates around a 5–10-day lag. Although the coherence is small, larger phase lags appear over parts of Sumatra and Java. Over western Borneo, Sulawesi, and New Guinea, the diurnal amplitude and MJO convection tend to be out of phase (i.e., enhanced diurnal amplitude under suppressed MJO convection), while the opposite phasing appears on the eastern side of the

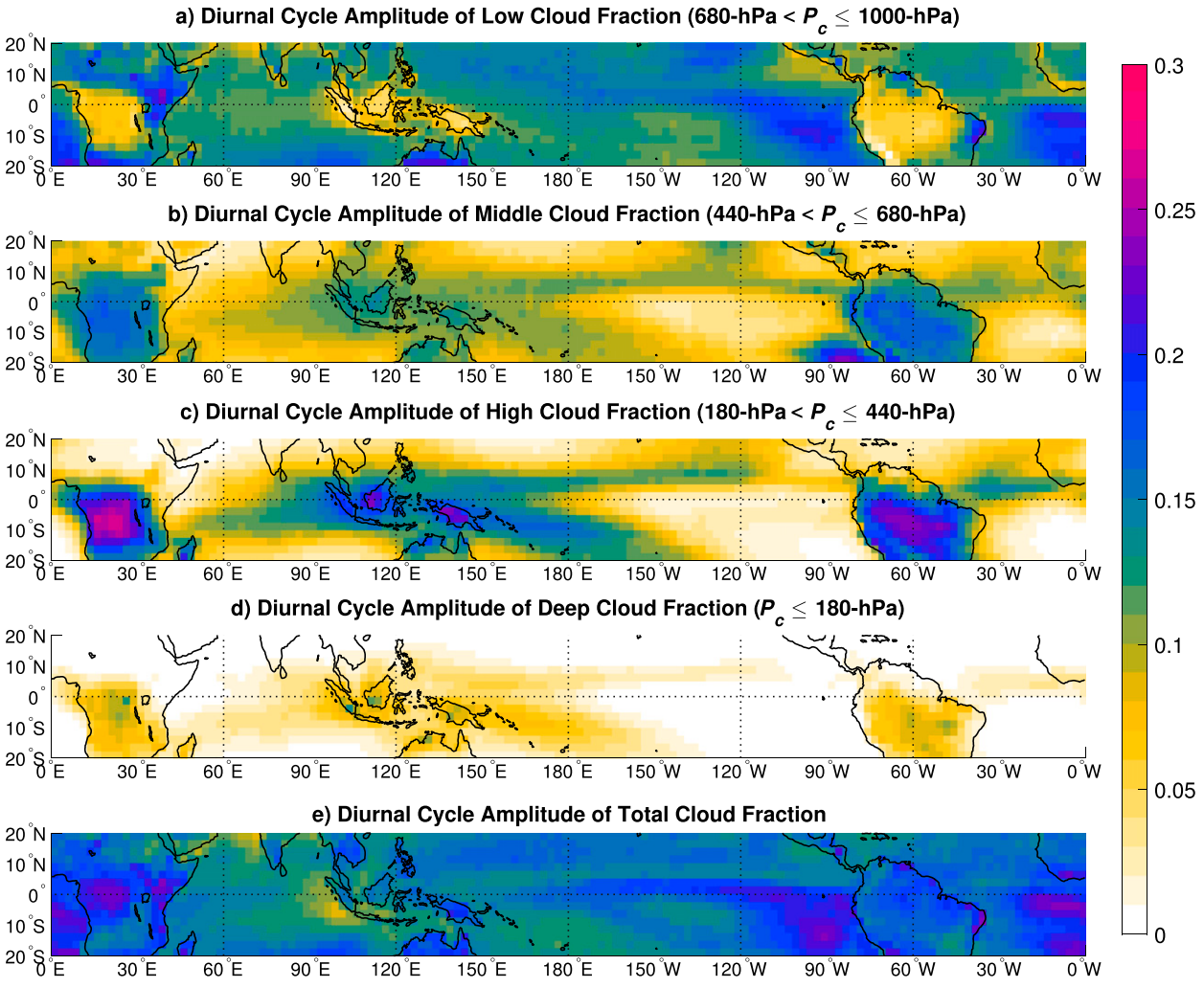

FIG. 3. As in Fig. 2, but showing the diurnal amplitude of cloud fraction.

islands. Using the RMM, Peatman et al. (2014) and Oh et al. (2012) similarly found that, over both land and ocean, the peak in the amplitude of the diurnal cycle leads the minimum in daily brightness temperature or the maximum in daily rainfall rate. However, the generally low coherence suggests that the relationship between the diurnal amplitude and MJO convection is not especially systematic over the islands of the MC, where the largest climatological diurnal cycle amplitudes are observed (Fig. 1b).

We also used the RMM and OLR MJO index (OMI; Kiladis et al. 2014) to composite the anomalous amplitude of rainfall diurnal cycle, as done in Peatman et al. (2014) and Oh et al. (2012). The OMI is an index similar to the RMM, but uses only filtered OLR to capture the global convective activity of the MJO. Using both the OMI and RMM, we again found that the composited amplitude of the diurnal cycle is not statistically significantly different from zero over most of the MC land (not shown). These results also support Fig. 5, which suggests that the relationship between MJO convection and diurnal amplitude over the MC islands is less systematic than that over the open ocean. Consistent with this result, Houze et al. (1981) and Kanamori et al. (2013) also showed that the MJO and other large-scale disturbances have a weaker effect on the diurnal cycle over the interior region of northwestern Borneo than in the coastal regions and surrounding ocean.

Figure 6 shows the coherence squared and phase between daily negative MJO-filtered OLR anomalies and the daily diurnal cycle amplitude of different cloud type fractions. The diurnal cycle amplitude of low cloud fraction varies most significantly over the MC and this tends to be out of phase there and elsewhere (Figs. 6a,b), indicating that the amplitude of the diurnal cycle of low cloud fraction tends to be at a minimum within the

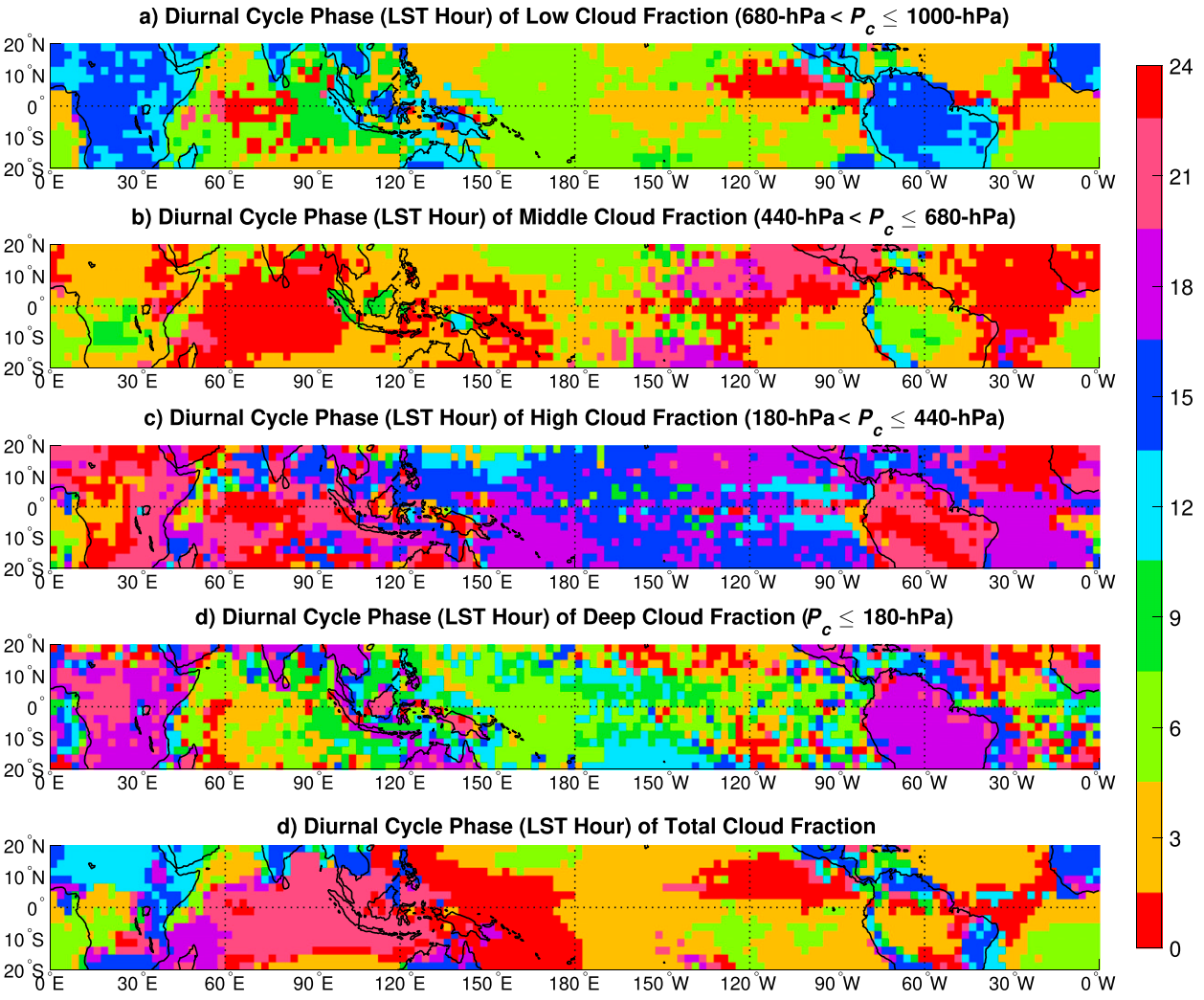

FIG. 4. As in Fig. 2, but showing the diurnal phase (LST hour) of cloud fraction.

convectively enhanced envelope of the MJO. The climatological diurnal peak of low clouds over land is at around 1200–1500 LST (Fig. 4), suggesting that isolated shallow cumulus clouds are initiated following thermal destabilization of the atmosphere from shortwave radiative heating of the surface (Yang and Smith 2006). The out-of-phase relationship with MJO convection (Fig. 6b) likely means that this destabilization is suppressed when enhanced MJO convection is present as a result of overall cloudier conditions. In addition, shallow clouds may be less detectable within enhanced MJO convection because of the more abundant higher clouds that overlie the low clouds, which could also lead to its weaker diurnal cycle signal. The diurnal cycle amplitude of middle–deep cloud fraction tends to increase within the enhanced envelope of the MJO over the ocean, as indicated by its strong coherence and near-zero phase lag (Figs. 6d–l). Similarly to the TRMM rainfall rate, the peak in the diurnal cycle amplitude of deep cloud tends to lead the negative peak in MJO-filtered OLR by a few days (Fig. 6k) near the coastlines.

The diurnal cycle amplitude must be zero on clear days; therefore, the inclusion of more clear days would lower the mean diurnal cycle amplitude during suppressed MJO convection. To test the impact of including clear-sky days, probability distributions of the amplitude of the diurnal cycle are compared between enhanced and suppressed MJO convection, using only days with a nonzero daily mean rainfall rate. Figures 7a and 7b show the distributions of TRMM 3B42 rainfall diurnal amplitude within MJO enhanced (blue) and suppressed (red) convection and all dates (climatology, black) during NDJFM over 15°N–15°S, 60°E–180°. Throughout the paper, when geographical averaging is used as in Fig. 7, these are weighted by grid cell area. The dots along the abscissa in Fig. 7 show mean values of diurnal

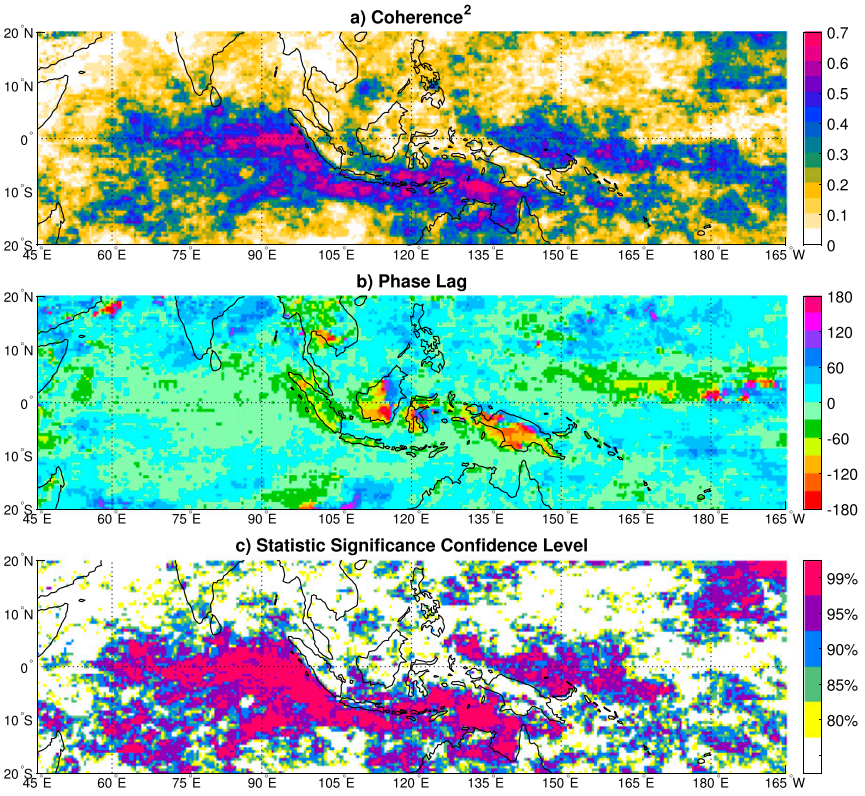

FIG. 5. Point-by-point (a) coherence squared and (b) phase (degrees) between daily MJO-filtered OLR anomaly and the diurnal amplitude of TRMM 3B42 rainfall rate during NDJFM. In (b), negative degree indicates that the diurnal amplitude leads negative MJO-filtered OLR and positive indicates the opposite. (c) Confidence level at where the coherence squared is statistically significantly different from noise.

cycle amplitude within each set. About 13.5% of the grid points are classified as land and 86.5% as ocean, and therefore the smaller sample size for land results in a wider confidence interval in Fig. 7. Differences in the distribution and mean value of the amplitude of the diurnal cycle of rainfall rate between enhanced and suppressed MJO convection are greater over ocean than land. Over land, the probability distribution within suppressed MJO convection differs only slightly from climatology, whereas over ocean the distribution clearly shifts to higher diurnal amplitude within enhanced MJO convection. The distributions over land become statistically indistinguishable between enhanced and suppressed MJO convection when coastal grid points are removed, indicating that the differences seen in Fig. 7a mostly come from coastal land (not shown). Similar changes in the distribution are found with daily mean rainfall rates (Figs. 7c,d) because the diurnal amplitude and daily mean value are highly correlated in time over the entire tropics (not shown).

Because the upper bound of diurnal amplitude is set by the daily mean value, an increase in diurnal amplitude does not necessarily mean that its ratio to the daily mean also increases. Figures 7e and 7f show the mean and probability distribution of the ratio of diurnal amplitude to daily mean TRMM rainfall rate. In contrast to the diurnal amplitude and daily mean (Figs. 7a–d), the ratio tends to be smaller within enhanced than suppressed MJO convection. This indicates that the increase in the diurnal cycle amplitude of rainfall rate from suppressed to enhanced MJO convection is smaller than the increase in the daily mean rainfall rate. The ratio of total variance explained by intradiurnal variability is also smaller within enhanced MJO convection than suppressed MJO convection (not shown).

Figure 8 shows similar probability distributions as in Figs. 7a and 7b for low, middle, high, and deep cloud fraction, excluding days with zero cloud fraction. Consistent with Fig. 6a, the mean value and distribution of low cloud fraction are significantly skewed toward lower values within enhanced compared to suppressed MJO convection over land (Fig. 8a), while no significant mean differences appear over ocean (Fig. 8b). However, the

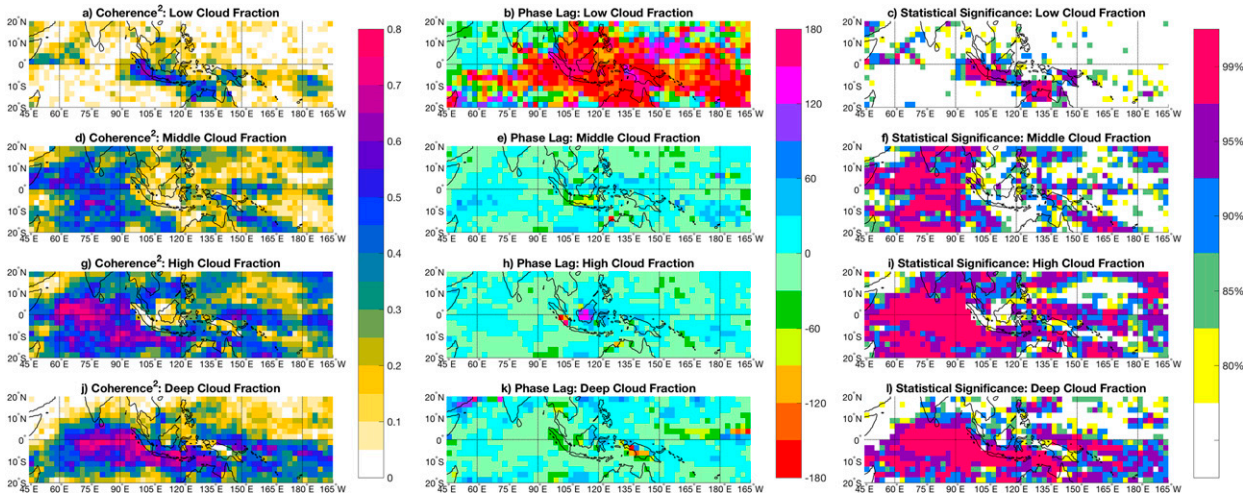

FIG. 6. Point-by-point (left) coherence squared and (middle) phase (degrees) between daily MJO-filtered OLR anomaly and ISCCP cloud fractions, and (right) confidence level at where the coherence squared is statistically significantly different from zero, for (a)–(c) low, (d)–(f) middle, (g)–(i) high, and (j)–(l) deep cloud fraction. Statistical significance is shown in the same manner as in Fig. 5. Gray crosses indicate points with not enough continuous data to apply cross-spectral analysis.

ratio of the diurnal cycle amplitude to the daily mean value of low cloud fraction is greater within enhanced than suppressed MJO convection (not shown), which means that the daily mean value of low cloud fraction decreases more significantly than its diurnal amplitude within enhanced MJO convection. For cloud fractions with higher cloud-top heights, the amplitude is greater within MJO enhanced convection (Figs. 8c,h) over both land and ocean. However, as with rainfall rates, the distribution difference over land between enhanced and suppressed MJO convection mostly comes from coastal land. In contrast to low cloud fraction, but similar to rainfall rate, the ratios of diurnal cycle amplitude to the daily mean value of cloud fraction with higher cloud tops are smaller within enhanced MJO convection (not shown), indicating that the daily mean value of the cloud fraction tends to increase at a greater rate than its diurnal amplitude from suppressed to enhanced MJO convection.

This section showed that diurnal variability of middle–deep cloud fraction and rainfall rate increases when transitioning from suppressed to enhanced MJO convection, and that the influence of the MJO on the diurnal variability is generally greater and more systematic over ocean than land. However, the rate of increase in the diurnal cycle amplitude from suppressed to enhanced MJO convection is smaller compared to the rate of increase in their daily mean rainfall rates. An exception is found with low cloud fraction, which tends to have a lower diurnal cycle amplitude within enhanced MJO convection and is more influenced by the MJO over land than ocean. This result suggests that driving mechanisms of the diurnal cycle of low, nonprecipitating clouds are different from precipitating deeper clouds. The same analysis was repeated by separating the basins into the Indian Ocean (60°–90°E), MC (90°–150°E), and western Pacific (150°E–180°) basins, and similar changes in the distribution and mean values of rainfall rate and cloudiness diurnal cycle amplitude with the MJO are found among these basins (not shown).

2) PHASE OF DIURNAL CYCLE

Figure 9 shows the probability distribution of the diurnal phase of rainfall rate over 15°N–15°S, 60°E–180°. Over both land and ocean, the mean and mode of the diurnal cycle phase do not change between enhanced and suppressed MJO convection, with both showing peaks in the afternoon over land and in the early morning over ocean. However, there are small but significant changes in the distribution. Over land, the diurnal peak becomes more frequent around midnight and less frequent between 1500 and 1800 LST within enhanced MJO convection, indicating a slight shift of the diurnal phase to later times compared to suppressed MJO convection. Over the ocean, the probability of peak diurnal rainfall decreases in the morning hours and increases in the early afternoon hours, implying that the timing of the diurnal cycle shifts to later times.

To better understand the changes in the probability distribution of the diurnal phase, Fig. 10 shows 3-hourly anomalous probability distributions of TRMM 3B42 rainfall rate, where the horizontal axis

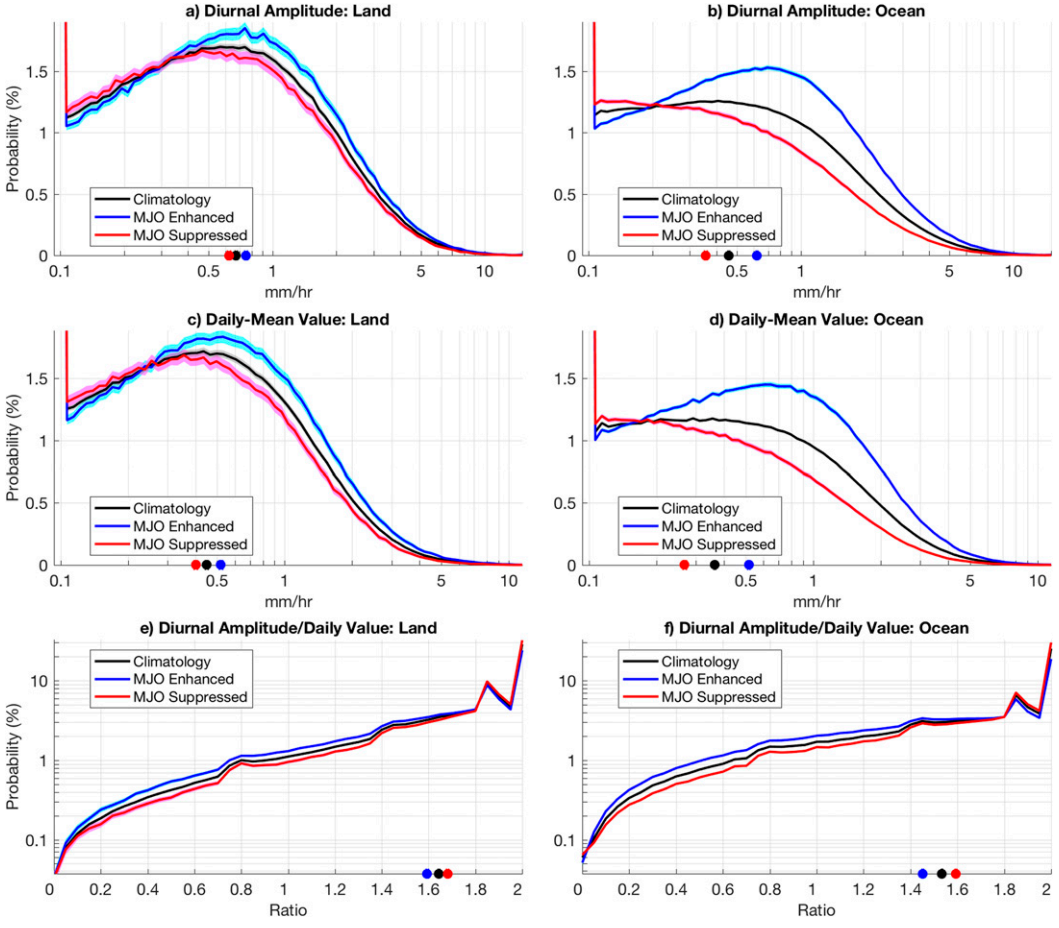

FIG. 7. Area-weighted probability distribution of (a),(b) diurnal cycle amplitude, (c),(d) daily mean value, and (e),(f) the ratio of diurnal amplitude to daily mean value over (left) land and (right) ocean over 15°N–15°S, 60°E–180° from TRMM 3B42 rainfall rate. Only days with nonzero precipitation are included. The black line shows the distribution of the NDJFM climatology, and red and blue lines show the distribution of days within enhanced and suppressed MJO convective envelopes. Gray, magenta, and cyan shading shows the 95% confidence interval for the NDJFM climatology and enhanced and suppressed MJO convection, respectively. The dots on the x axis show the mean value within the three sets using their corresponding line colors. The 95% confidence intervals only appear when they are greater than the size of the dots.

represents LST and the vertical axis represents rainfall rate. In Fig. 10, the black line plot on the left shows probability distributions of rainfall rates from all hours [i.e., daily distribution, $F^d(x)$] as calculated in (1), where $N(h, x)$ is the number of data points in each 3-hourly bin of LST hour h ($H = 8$) and rainfall rate bin on a natural log scale x, where X is the number of bins:

$$F^d(x) = \sum_{h=1}^{H} N(h,x) \Big/ \sum_{h=1}^{H} \sum_{x=1}^{X} N(h,x). \qquad (1)$$

The shading in Fig. 10 shows the anomalous probability distribution of rainfall rate $F'(h, x)$ at each 3-hourly LST from the daily probability distribution:

$$F'(h,x) = \left[N(h,x) \Big/ \sum_{x=1}^{X} N(h,x) \right] - F^d(x). \qquad (2)$$

To calculate the anomalous probability, the distribution is normalized by the number of data points within each 3-hourly bin, since this can differ, especially in TRMM 3G68 data. The bin with the smallest rain rate includes zero rain rates, so it primarily represents the frequency of no rain occurrences. These anomalous probabilities show the hour at which the occurrence of rain rates becomes more or less frequent than its daily probability. The black line plot across the top in Fig. 10 shows the mean rainfall rate in each 3-hourly LST bin. Figures 10e and 10f) show the difference in each plotted quantity

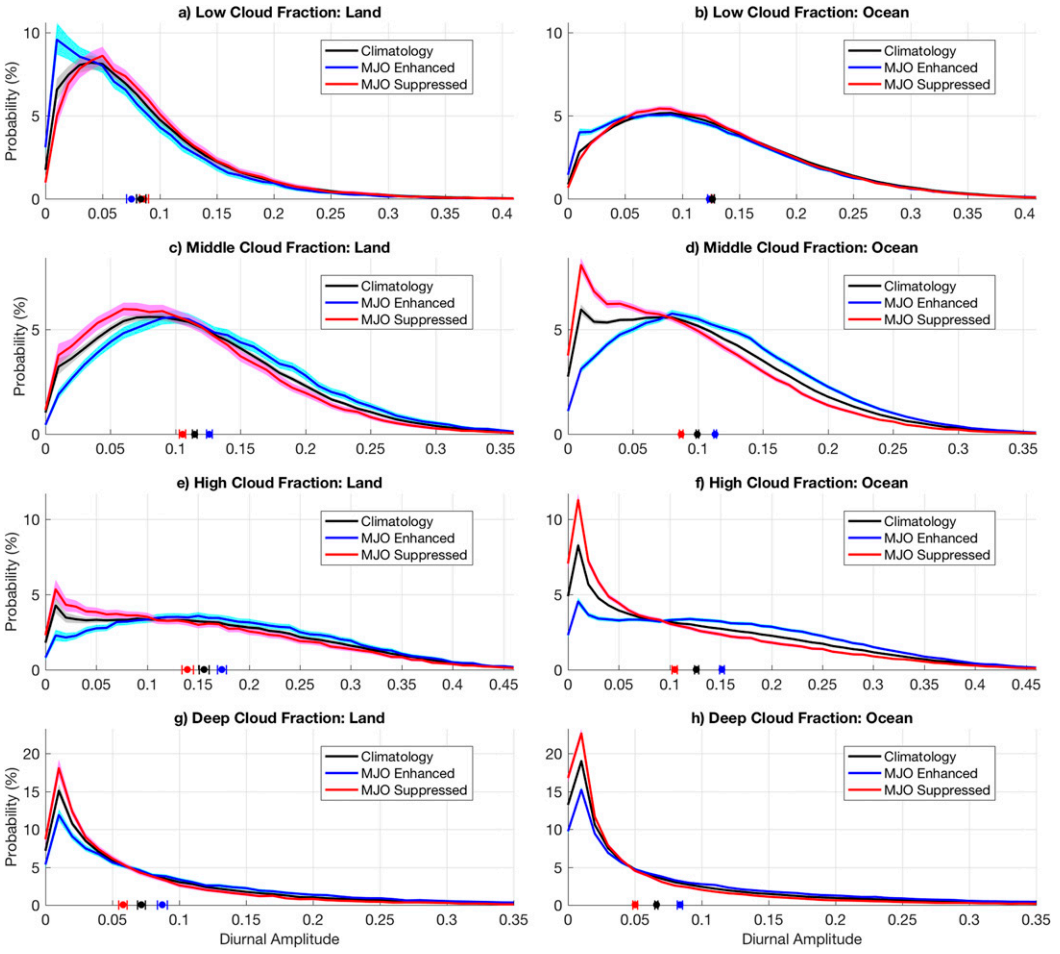

FIG. 8. As in Fig. 7, but showing the diurnal cycle amplitude of (a),(b) low, (c),(d), middle, (e),(f) high, and (g), (h) deep cloud fraction.

between enhanced and suppressed MJO convection (note change in scale). The anomalous probability and its difference are only shaded where they are significantly different from zero at the 95% confidence level; otherwise, they appear white. Positive differences in the anomalous probability indicate that the difference at those hours is greater than the difference in daily probability.

Over land (Figs. 10a,c), rainfall becomes more frequent after noon and increases in amplitude toward the evening. The general diurnal patterns are similar between enhanced (Fig. 10a) and suppressed (Fig. 10c) MJO convection, but the difference between the two (Fig. 10e) shows that the probability of rainfall becomes higher around midnight during enhanced MJO convection (Kanamori et al. 2013). This more frequent rainfall around midnight contributes to the shifts in the distribution of diurnal cycle phase (Fig. 9a). The strongest rainfall rates (above 10 mm h^{-1}) around midnight tend to occur over coastal land, but midnight rainfall still becomes more frequent inland (not shown). Ichikawa and Yasunari (2006, 2008) also showed that the convective rain that initiates inland of MC islands around afternoon tends to propagate faster toward coastlines and enhance coastal rainfall around midnight during enhanced MJO convective phases.

Over the ocean (Figs. 10b,d), rainfall at all rates is most frequent around 0600 LST, and the strong rainfall rate that peaks around 0600 LST gradually decays toward late afternoon. This gradual decrease in the amplitude of rainfall rate from early morning into afternoon is less apparent during suppressed MJO convection (Fig. 10d). Strong rainfall rates (above 5 mm h^{-1}) are further concentrated during the morning hours (0300–0900 LST) during enhanced MJO convection (Fig. 10f), but the largest difference in the probability between the enhanced and suppressed MJO convection occurs at moderate rainfall rates (1–5 mm h^{-1}) in the

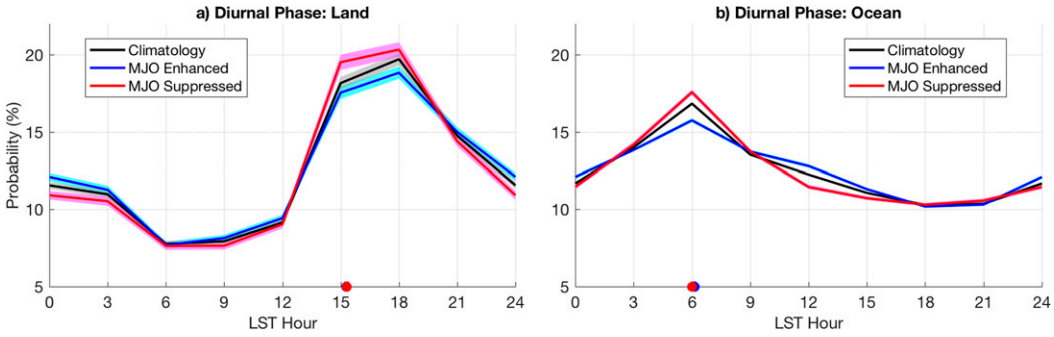

FIG. 9. As in Fig. 7, but showing the probability distribution of daily diurnal phase (LST hours).

afternoon. This more frequent moderate rain in the afternoon results in the shift of the diurnal phase distribution in Fig. 9b. This shift is also consistent with Oh et al. (2012) and Rauniyar and Walsh (2011), who showed a slight delay in the diurnal phase within enhanced MJO convection. However, since the hours of maximum probability of strong rainfall rate do not vary as much, the diurnal peak of the mean rainfall rate remains at 0600 LST regardless of the phase of the MJO (top black lines of Figs. 10b,d).

As mentioned in the introduction, there is disagreement in a number of previous studies on whether the MJO has an effect on the diurnal phase of rainfall. The results presented here suggest that this may be due to the parameters studied and the methods of analysis. For example, past studies that have examined the average diurnal cycle (Tian et al. 2006; Suzuki 2009) or deep cloud fraction (Tian et al. 2006) concluded that the MJO does not significantly impact diurnal phase. On the other hand, some changes in the diurnal phase of rainfall with the MJO were found by other studies that examined the diurnal cycle through probability distributions or modal decomposition such as empirical orthogonal function analysis (Chen and Houze 1997; Fujita et al. 2011; Oh et al. 2012; Rauniyar and Walsh 2011). The results of this study show that the mean diurnal phase does not vary much with the MJO, but the MJO influences the probability distribution of the diurnal phase. The overall probability distribution of rainfall rates between enhanced and suppressed MJOs are similar, with differences amounting only to a few percent. However, the differences are statistically significant, suggesting that there are subtle but significant changes in the diurnal cycle of rainfall and cloud populations with the MJO.

The same two-dimensional probability distributions of rainfall rate as in Fig. 10 were generated from TRMM 3G68 PR rainfall rate (Fig. 11). Over both land and ocean, the diurnal peak in probability and mean rainfall rates tend to occur about 3 h earlier in the TRMM 3G68 PR than the 3B42 data, as documented by other studies (discussed in section 3a). Although there is a slight phase lag in the diurnal cycle, the TRMM 3G68 PR data also shows an afternoon maximum in rainfall over land and early morning maximum over the ocean. The distribution is noisier in the TRMM 3G68 PR data because of its smaller sample size (about 5% of the TRMM 3B42 sample size), especially over land. Over the ocean, the difference between enhanced and suppressed MJOs (Fig. 11f) shows a similar pattern as in TRMM 3B42 data (Fig. 10f), with increased probability of strong rainfall rates in the early morning hours and of moderate–weak rainfall rates in the afternoon. The mean diurnal cycle within MJO enhanced and suppressed phases (top black lines in Figs. 11b,d) shows a 3-h difference in timing when compared to the TRMM 3B42 data. This amounts to a peak at 0600 LST during enhanced and at 0300 LST during suppressed MJO convection, whereas the peak appears at 0600 LST during both phases from the TRMM 3B42 data (Fig. 10). This contrast between TRMM 3B42 and 3G68 PR data suggests that the changes in the diurnal cycle with the MJO are better captured by more sensitive and higher-resolution instruments such as the TRMM PR.

To compare the diurnal cycle of rainfall rate to cloud fraction, Fig. 12 shows the 3-hourly mean fraction of clouds at each resolved cloud-top pressure from ISCCP. In Fig. 12, the black line on the left shows the daily mean fraction of clouds at each cloud-top pressure while the mean cloud fraction anomaly from its daily mean value is shaded. Consistent with Fig. 2, the fraction of high clouds is greater over land than ocean, with more abundant low cloud over the ocean. Over both land and ocean, daily mean fraction of middle–deep cloud increases while low cloud decreases within enhanced MJO convection (Figs. 12e,f).

Over land, high and deep cloud fractions tend to peak from the late evening to midnight, followed by a decrease in cloud-top height through morning into afternoon, leading to the maximum low cloud fraction in

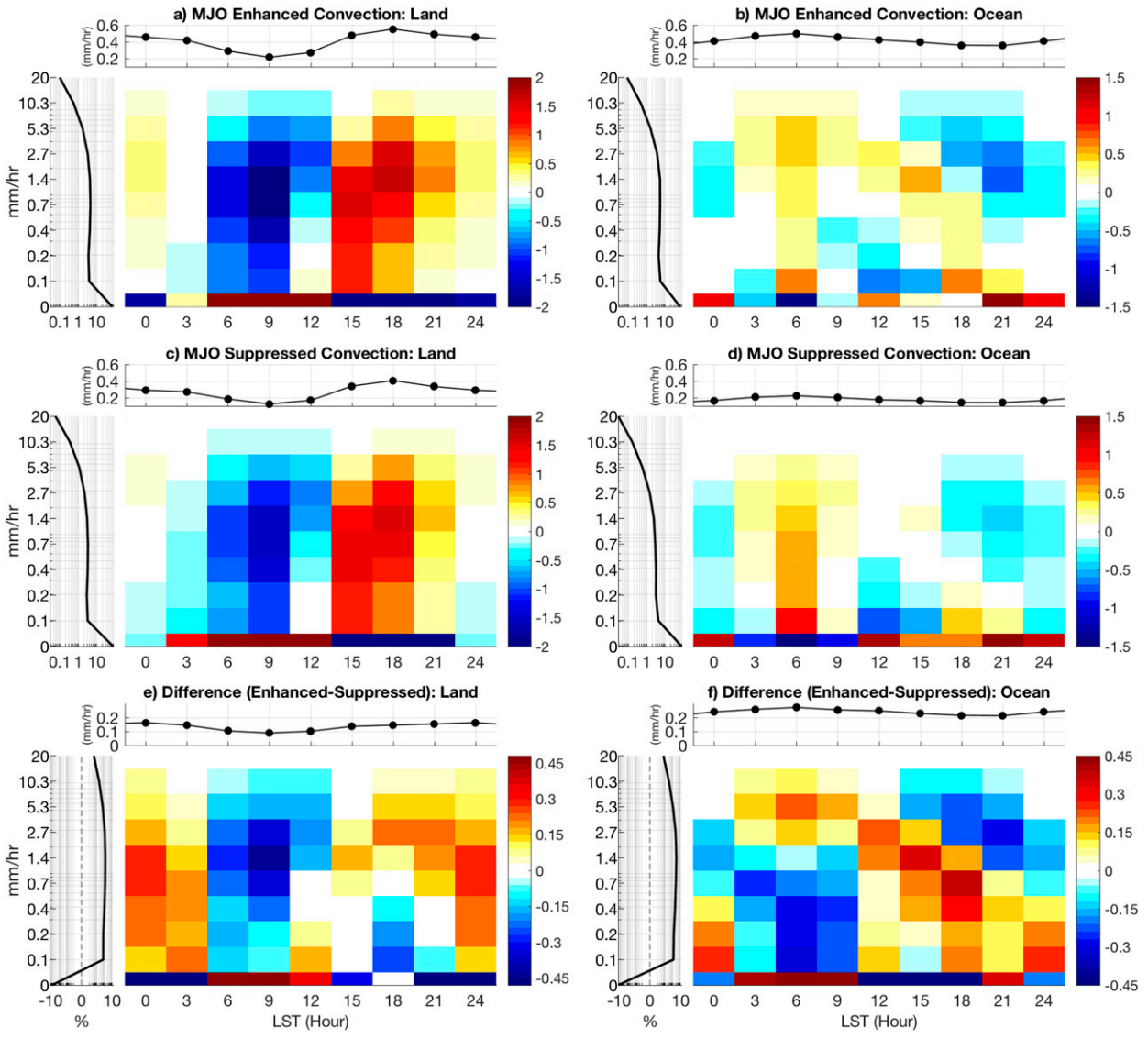

FIG. 10. The black line plot across the top shows mean rainfall rate (mm h^{-1}) at each 3-hourly LST. The shading shows the diurnal anomalous probability distribution (%) of TRMM 3B42 rainfall rate at each 3-hourly LST, where the horizontal axes show 3-hourly LST and the vertical axes show rainfall rates on a natural logarithmic scale. The black line plot on the left shows the probability distribution (%, horizontal axis) of rainfall rate from all hours of day, where the probability is plotted on natural logarithmic scale. Shown are days within MJO (a),(b) enhanced and (c),(d) suppressed convection and (e),(f) the difference between enhanced and suppressed convection over 15°N–15°S, 60°E–180°, over (left) land and (right) ocean. The diurnal anomalous probability is only shaded in color (i.e., nonwhite) if the diurnal anomaly in (a)–(d) or the differences in (e) and (f) are significantly different from zero at 95% confidence level.

early afternoon (consistent with Fig. 4). The difference between enhanced and suppressed MJO convection over land shows increased high cloud fraction around midnight within enhanced MJO convection, perhaps associated with the rainfall peaks around midnight shown in Figs. 10 and 11. Middle cloud fraction also increases between late morning and noon within enhanced MJO convection, suggesting a slower decay time of the high clouds that peak in the evening in Fig. 12.

Over the ocean, deep cloud fraction peaks in the morning, followed by a decrease in cloud-top height throughout the afternoon and evening into morning. The period of this decay in cloud-top height is slower over ocean than land, as is also reflected in the climatology (Fig. 4). Figure 12f shows an increase in the diurnal amplitude of deep and high cloud fraction within enhanced MJO convection, and a slight slowdown in the decay time of cloud heights. These changes in cloud

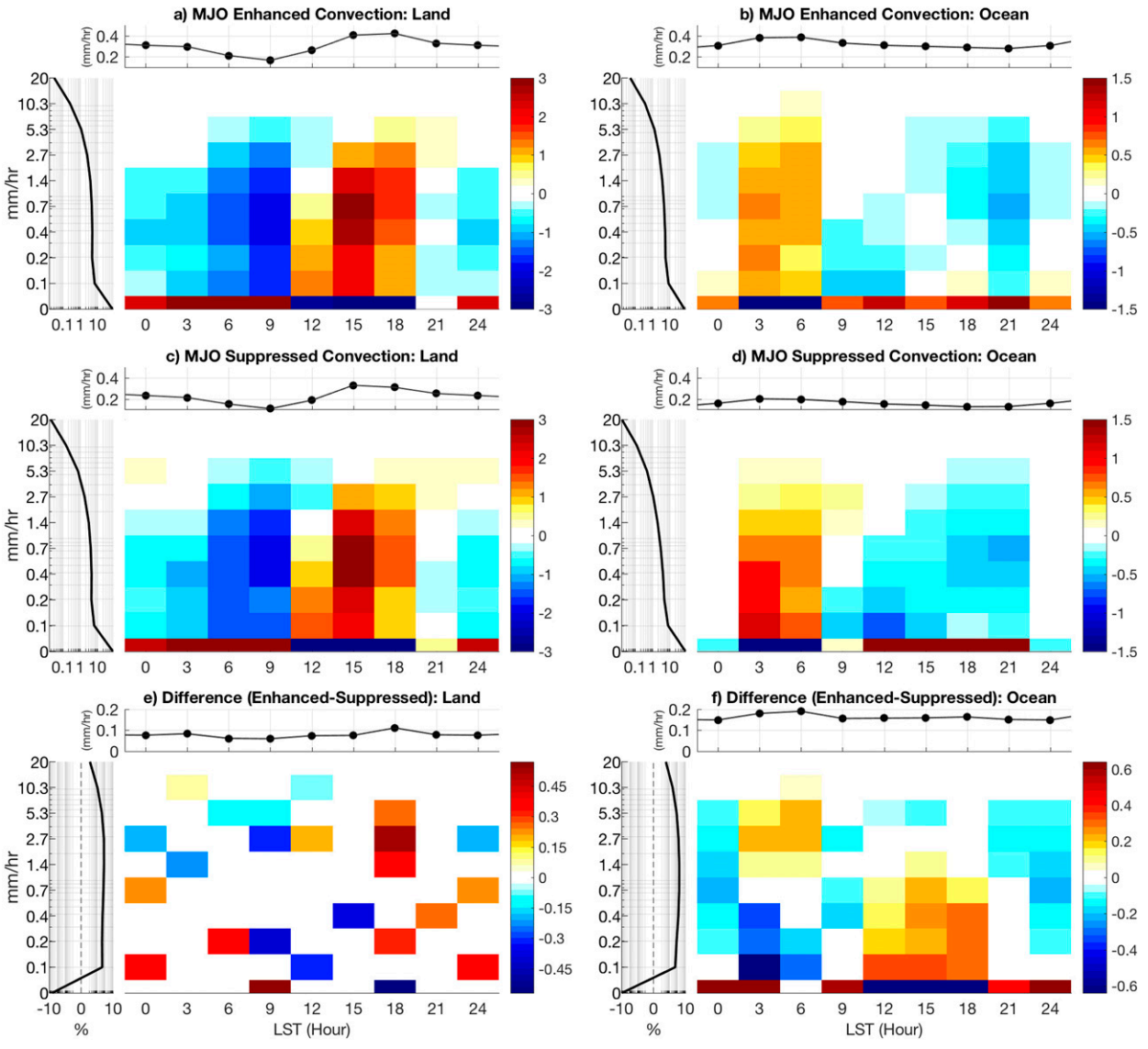

FIG. 11. As in Fig. 10, but using TRMM 3G68 PR rainfall rate (mm h^{-1}).

fraction indicate that more oceanic deep clouds in the morning within the enhanced MJO is associated with higher rainfall rates and the subsequent increase in high clouds in the afternoon is associated with greater moderate rainfall rates then (Figs. 10f and 11f). Middle and low cloud fractions also increase in late morning to noon within enhanced MJO convection, suggesting a slower decay time of cloud-top height or increased formation of the shallower clouds induced by downdrafts of deep convective clouds (Feng et al. 2015; Ruppert and Johnson 2015; Rowe and Houze 2015). However, it is difficult to distinguish decaying clouds and newly forming clouds from the diagnostics used here. These changes in the diurnal variability of cloudiness and rainfall rate between enhanced and suppressed MJO convection are also found when the Indian Ocean, MC, and western Pacific basins are examined separately.

3) DIURNAL CYCLE OF RAIN CHARACTERISTICS

This section further examines the diurnal cycle of rain characteristics using TRMM 3G68 PR data. Despite the disadvantages of a smaller sample size, TRMM 3G68 data allow a more detailed analysis of the factors contributing to diurnal cycle changes. The rainfall rates presented in previous sections are the areal mean rates at each grid cell R, which can be represented as the product of conditional rainfall rate R_c and raining area fraction A_r:

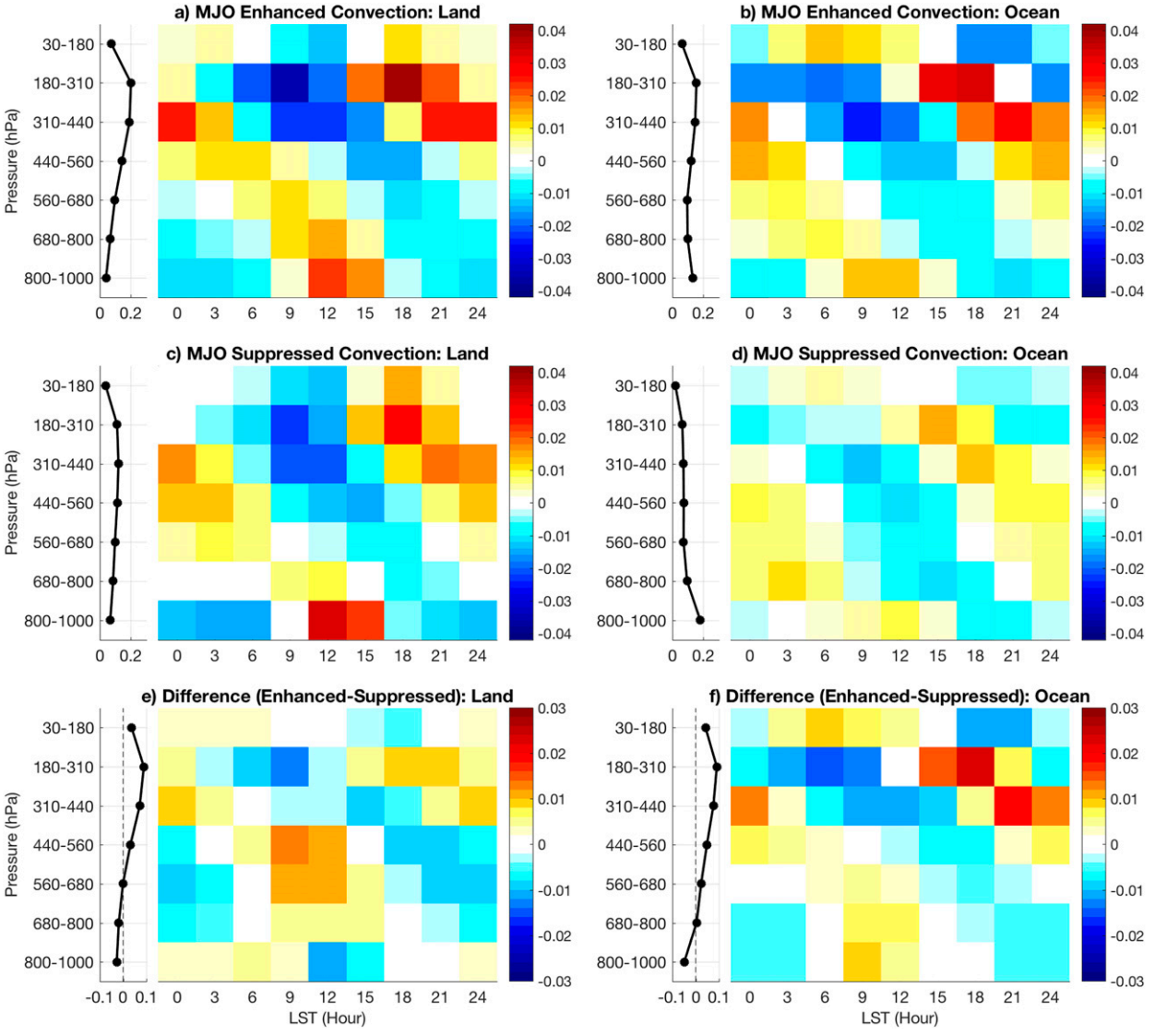

FIG. 12. As in Figs. 10 and 11, but shading shows the diurnal anomaly of mean cloud fraction at each cloud-top pressure and 3-hourly LST and the black line plot on the left shows the mean cloud fraction at each cloud-top pressure at all hours of the day.

$$R = R_c A_r. \tag{3}$$

Raining area fraction is calculated as the ratio of the number of raining pixels to total pixels within a grid cell. The conditional rainfall rate is defined as the mean rainfall rate within raining pixels, which is a better estimate of the intensity of rainfall. The areal-mean and conditional rainfall rates are further decomposed to convective R^{conv} and nonconvective R^{strat} (mostly stratiform):

$$R = R^{\text{conv}} + R^{\text{strat}} = (R_c^{\text{conv}} + R_c^{\text{strat}})A_r. \tag{4}$$

Figure 13 shows the average diurnal time series of decomposed rainfall rates within enhanced (solid lines) and suppressed (dashed lines) MJO convection. As discussed previously, Figs. 13a,b show that overall rainfall rates are increased within the MJO and there is a 3 hourly delay in the peak rainfall, especially evident over land. Over both land and ocean, raining area fraction A_r (Figs. 13i,j) peaks at the same hour as the areal mean rainfall R (Figs. 13a,b), while the conditional rainfall rate R_c (Figs. 13e,f) leads by about 3 h, indicating that the raining area fraction dominates the diurnal variability (Nesbitt and Zipser 2003; Biasutti et al. 2012).

Over land, more than 50% of the diurnal peak in the afternoon is from convective rainfall, while the stratiform and convective rainfall contribute more equally around midnight (Fig. 13c). Within enhanced MJO

convection, the stratiform contribution increases from evening through early morning, and it even exceeds the convective rainfall from 0000 to 0900 LST. Therefore, more frequent weak rainfall around midnight within MJO enhanced convection over land (Figs. 10 and 11) is associated with an increase in stratiform rain. Conditional rainfall tends to peak about 3 h earlier than raining area fraction because conditional rainfall is more dominated by convective rain that peaks around 1500 LST, while raining area fraction is dominated by stratiform rain that broadly maximizes from 1800 to 0300 LST.

Over ocean, in contrast to land, convective and stratiform rain contribute more equally to the total areal-mean rainfall at all hours, but stratiform-to-convective ratio increases within enhanced MJO convection (Fig. 13d), as shown by previous studies (Barnes and Houze 2013; Zuluaga and Houze 2013; Xu and Rutledge 2014; Powell and Houze 2015). The conditional rainfall rate has small diurnal variability (Nesbitt and Zipser 2003; Biasutti et al. 2012) but it tends to peak around 0000–0300 LST (Fig. 13f) while raining area fraction peaks around 0300–0600 LST (Fig. 13j). This is again because total conditional rainfall rate tends to be dominated by convective rain that peaks around 0000–0300 LST while raining area fraction is dominated by stratiform rain that peaks around 0600–0900 LST (Fig. 13h). The peak of stratiform rain following convective rain suggests that the stratiform rain tends to develop as anvil clouds associated with deep convection within mesoscale convective systems (Houze et al. 1981). Therefore, more abundant stratiform rainfall within enhanced MJO convection leads to the slightly delayed peak of total areal-mean or conditional rainfall rate (Figs. 13b,f) and the shift in the probability distribution of the diurnal phase (Figs. 9–11).

4. Summary and discussion

This study examines the tropical diurnal cycle of cloudiness and rainfall and its variability associated with MJO convection using TRMM rainfall rate and ISCCP cloud fraction data during November–March for 1998 through 2009. As has been shown in past studies, we found that the climatological characteristics of the diurnal cycle in rainfall and cloudiness differ greatly between land and ocean and they also vary locally with respect to the presence or absence of the MJO. The amplitude of the diurnal cycle of rainfall generally increases within the envelope of enhanced MJO convection and decreases within regions of suppressed MJO convection, and this signal is especially prominent over the ocean. Over the islands of the MC near coastlines, the amplitude of the diurnal cycle tends to increase 5–10 days prior to the arrival of minimum OLR associated with the MJO, however the coherence between the diurnal cycle amplitude and MJO-filtered OLR is weak over most of the islands, where the climatological diurnal cycle amplitude is large (Houze et al. 1981; Kanamori et al. 2013). The phase relationship between the diurnal amplitude and MJO convection also varies geographically over MC islands. Previous studies also found some relationship between the MJO and diurnal rainfall rate over the islands of the MC (Ichikawa and Yasunari 2006, 2008; Oh et al. 2012; Rauniyar and Walsh 2011; Peatman et al. 2014). However, the statistical tests shown here suggest that such relationships appear to be statistically insignificant, especially away from the coasts. The reason for this less systematic relationship between the MJO and diurnal cycle over the islands of the MC is not clear, but it suggests that their interactions are complicated by land–sea effects and topography.

The diurnal cycle amplitudes of middle, high, and deep cloud fractions also increase within enhanced MJO convection, again especially over the ocean. In contrast, the diurnal amplitude of low cloud fraction decreases within enhanced MJO convection and this change tends to be stronger over land. In general, the diurnal cycle amplitude of rainfall rate and cloudiness increase from suppressed to enhanced MJO convection when their daily mean values also increase. However, the change in diurnal cycle amplitude between suppressed and enhanced MJO convection is often smaller than the change in daily mean values. In other words, while the diurnal cycle amplitude increases from suppressed to enhanced MJO convection, its ratio to the daily mean value decreases. Conversely, the diurnal cycle amplitude of low clouds decreases within enhanced MJO convection, while its ratio to the daily mean value increases. Therefore, even though the amplitude of the diurnal cycle becomes greater within enhanced MJO convection, its relative contribution to total rainfall or cloudiness variance within MJO convection becomes smaller, except for the case of low clouds. The MJO also influences the phasing of the diurnal cycle in rainfall rate and cloudiness. Over land, rainfall peaks more frequently around midnight within enhanced MJO convection, especially near coastlines, because of an increased areal extent of stratiform rain. The modulation of the diurnal phasing over the islands of the MC by the MJO is also geographically dependent (see also Ichikawa and Yasunari 2006, 2008; Fujita et al. 2011).

The schematic in Fig. 14 summarizes how the diurnal cycle varies with the MJO over the ocean. Within enhanced MJO convection, the peak in rainfall rate during the early morning hours is followed by moderate–weak

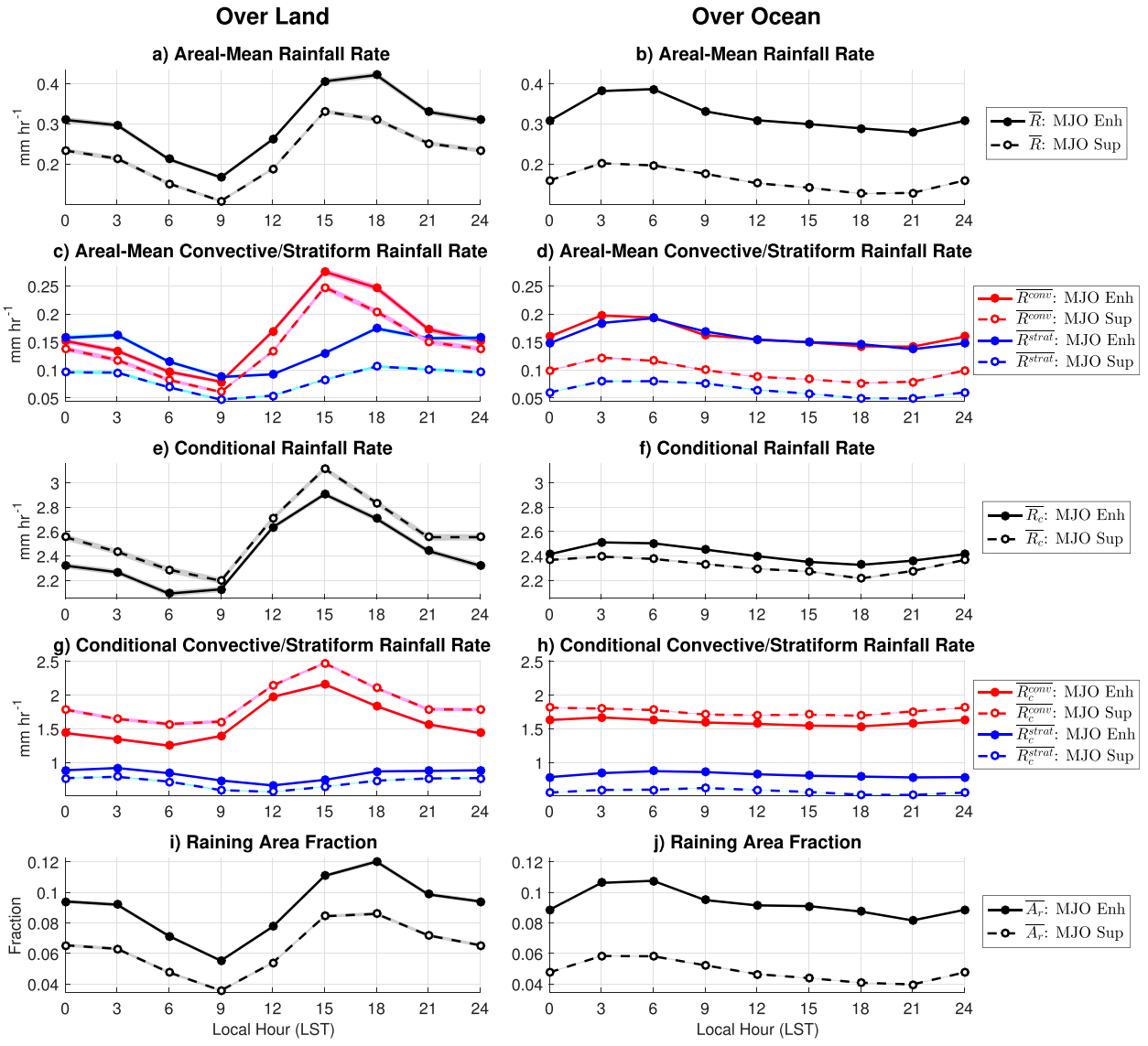

FIG. 13. Average diurnal time series of (a),(b) areal-mean, (c),(d) areal-mean convective (red) and stratiform (blue), (e),(f) conditional, and (g),(h) conditional convective (red) and stratiform (blue) rainfall rates (mm h^{-1}) and (i),(j) raining area fraction within enhanced (solid lines) and suppressed (dashed lines) MJO convection.

rainfall rates becoming more frequent in the afternoon and evening resulting from an increase in stratiform rain. The more frequent occurrence of organized convection within the MJO leads to increased formation of stratiform anvil clouds, which have greater horizontal extent than convective clouds and contribute largely to the areal mean rainfall rates (Barnes and Houze 2013; Zuluaga and Houze 2013; Xu and Rutledge 2014; Powell and Houze 2015). The less frequent occurrence of stratiform rain within suppressed MJO convection results in a shift of the diurnal rainfall peak to earlier hours of the day. These changes lead to more frequent diurnal peaks occurring a few hours later within enhanced MJO convection over the ocean. However, since strong rainfall rates are still concentrated in the early morning, the mean diurnal rainfall rate retains its maximum in those hours in TRMM 3B42 data (Fig. 10), while a change in the mean appears in TRMM 3G68 PR data (Fig. 11). Although the diurnal peak occurs more frequently at a later time of day, the mean and mode of the diurnal phase do not vary significantly with the MJO in TRMM 3B42 data. Furthermore, the variability in the phase of diurnal cycle with the MJO also depends on the exact parameter in question. Strong rainfall rates and deep convective cloud fraction peak during the early morning hours in both phases of the MJO, which has led some

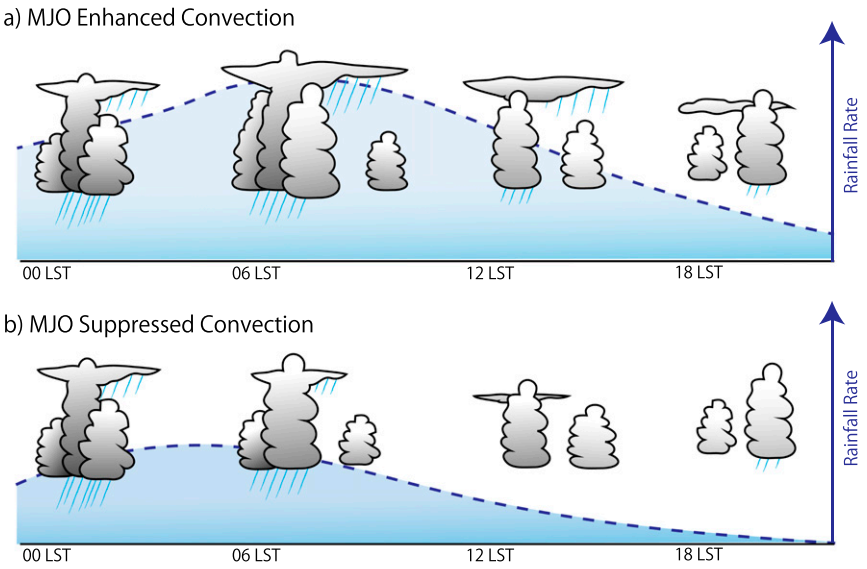

FIG. 14. Schematic of the diurnal cycle over the tropical open ocean during (a) enhanced and (b) suppressed MJO convection. Convective and stratiform rain is represented by the rain at the bottom of convective towers and anvils, respectively. The dotted blue line represents the mean diurnal rainfall rate.

previous studies to conclude that the MJO has no influence on the phase of diurnal cycle (Tian et al. 2006; Suzuki 2009). However, more variability in the diurnal distribution occurs with low–middle cloud fraction and moderate–weak rainfall rates between enhanced and suppressed MJO convection because of changes in the cloud population. Other studies that have examined the variability and distribution of the diurnal cycle, as done in this study, concluded that the MJO has some influence on the phase of diurnal cycle (Chen and Houze 1997; Fujita et al. 2011; Oh et al. 2012; Rauniyar and Walsh 2011).

In contrast to the open ocean, the relationship between the MJO and the diurnal cycle is more complicated within the MC. The diurnal evolution of cloudiness and rainfall over the MC varies geographically depending on topography and associated diurnal land–sea and mountain–valley breezes and cloud-induced gravity waves (Mori et al. 2004; Sakurai et al. 2005; Keenan and Carbone 2008; Biasutti et al. 2012; Hassim et al. 2016). Interactions between the MJO and the diurnal cycle over the MC have been hypothesized to influence the propagation of the MJO (Slingo et al. 2003; Peatman et al. 2014; Hagos et al. 2016). However, the geographic variability of the relationship between the MJO and the diurnal cycle suggests that in-depth studies on regional scales are necessary (e.g., island by island) to understand the potential role of the diurnal cycle on MJO propagation. Our study also suggests that the behavior of the diurnal cycle over the MC islands has large event-to-event variability (Fig. 5), which may be important for understanding different propagation characteristics of individual MJOs (Jones et al. 2004; Kerns and Chen 2016).

While this study provides insights into the characteristics and variability of the diurnal cycle of cloudiness and rainfall associated with the MJO, further analyses are required to understand the physical mechanisms behind the variability of the diurnal cycle of rainfall and cloud type populations. Sui et al. (1997) and Ruppert and Johnson (2015) observed the formation of clouds following the warming of SST in the afternoon, especially within suppressed MJO convection, yet such a development of cloudiness or rainfall is not well detected in this study. This discrepancy may be due to the difference in event sample size, geographical location, or instrument resolution (ground-based radar vs satellites) since the resolution of TRMM is known to be too coarse to capture small-scale rain (Tabata et al. 2011). Using a high-resolution regional model, Birch et al. (2016) showed that the diurnal land–sea contrast over Sumatra depends on the modulation of incoming solar radiation, moisture, and surface fluxes that are associated with the MJO. While some mechanisms of how the MJO could impact the diurnal cycle over the MC islands have been proposed (Ichikawa and Yasunari 2008; Oh et al. 2012; Peatman et al. 2014; Birch et al. 2016), how this modulation occurs over the open ocean is less clear. The roles of moisture, radiation, large-scale circulation, and cloud life cycles, along with their interactions, need to be examined in greater detail to understand the physical mechanisms that

drive the diurnal cycle and its geographical variability. Another important question to be addressed in the future is whether the changes in the characteristics of diurnal cycle feed back and play a role in MJO initiation or evolution.

Acknowledgments. We thank Maria Gehne for her help in preparing data used in this study. ISCCP Cloud fraction data were obtained from the NASA Langley Research Center Atmospheric Data Center. Discussions with Stefan Tulich and Brian Mapes were especially helpful for clarifying the role of MJO enhanced rainfall in the diurnal cycle amplitude changes. Constructive comments from three anonymous reviewers were also very helpful in crystallizing ideas and in improving the text. This research was performed while the first author held an NRC Research Associateship award at NOAA. We gratefully acknowledge support for this work through Grant NA13OAR4310165 from the Climate Program Office at NOAA.

REFERENCES

Albright, M. D., E. E. Recker, R. J. Reed, and R. Dang, 1985: The diurnal variation of deep convection and inferred precipitation in the central tropical Pacific during January–February 1979. *Mon. Wea. Rev.*, **113**, 1663–1680, doi:10.1175/1520-0493(1985)113<1663:TDVODC>2.0.CO;2.

Amante, C., and B. W. Eakins, 2009: ETOPO1 1 arc-minute global relief model: Procedures, data sources and analysis. NOAA Tech. Memo. NESDIS NGDC-24, 19 pp. [Available online at https://www.ngdc.noaa.gov/mgg/global/relief/ETOPO1/docs/ETOPO1.pdf.]

Augustine, J. A., 1984: The diurnal variation of large-scale inferred rainfall over the tropical Pacific Ocean during August 1979. *Mon. Wea. Rev.*, **112**, 1745–1751, doi:10.1175/1520-0493(1984)112<1745:TDVOLS>2.0.CO;2.

Barnes, H. C., and R. A. Houze, 2013: The precipitating cloud population of the Madden–Julian oscillation over the Indian and west Pacific Oceans. *J. Geophys. Res. Atmos.*, **118**, 6996–7023, doi:10.1002/jgrd.50375.

Bernie, D. J., E. Guilyardi, G. Madec, J. M. Slingo, S. J. Woolnough, and J. Cole, 2008: Impact of resolving the diurnal cycle in an ocean–atmosphere GCM. Part 2: A diurnally coupled CGCM. *Climate Dyn.*, **31**, 909–925, doi:10.1007/s00382-008-0429-z.

Biasutti, M., S. E. Yuter, C. D. Burleyson, and A. H. Sobel, 2012: Very high resolution rainfall patterns measured by TRMM Precipitation Radar: Seasonal and diurnal cycles. *Climate Dyn.*, **39**, 239–258, doi:10.1007/s00382-011-1146-6.

Biello, J. A., and A. J. Majda, 2005: A new multiscale model for the Madden–Julian oscillation. *J. Atmos. Sci.*, **62**, 1694–1721, doi:10.1175/JAS3455.1.

Birch, C. E., S. Webster, S. C. Peatman, D. J. Parker, A. J. Matthews, Y. Li, and M. E. E. Hassim, 2016: Scale interactions between the MJO and the western Maritime Continent. *J. Climate*, **29**, 2471–2492, doi:10.1175/JCLI-D-15-0557.1.

Cairns, B., 1995: Diurnal variations of cloud from ISCCP data. *Atmos. Res.*, **37**, 133–146, doi:10.1016/0169-8095(94)00074-N.

Chen, S. S., and R. A. Houze, 1997: Diurnal variation and life-cycle of deep convective systems over the tropical Pacific warm pool. *Quart. J. Roy. Meteor. Soc.*, **123**, 357–388, doi:10.1002/qj.49712353806.

Dai, A., 2001: Global precipitation and thunderstorm frequencies. Part II: Diurnal variations. *J. Climate*, **14**, 1112–1128, doi:10.1175/1520-0442(2001)014<1112:GPATFP>2.0.CO;2.

——, X. Lin, and K.-L. Hsu, 2007: The frequency, intensity, and diurnal cycle of precipitation in surface and satellite observations over low- and mid-latitudes. *Climate Dyn.*, **29**, 727–744, doi:10.1007/s00382-007-0260-y.

Deser, C., and C. A. Smith, 1998: Diurnal and semidiurnal variations of the surface wind field over the tropical Pacific Ocean. *J. Climate*, **11**, 1730–1748, doi:10.1175/1520-0442(1998)011<1730:DASVOT>2.0.CO;2.

Dias, J., S. Leroux, S. N. Tulich, and G. N. Kiladis, 2013: How systematic is organized tropical convection within the MJO? *Geophys. Res. Lett.*, **40**, 1420–1425, doi:10.1002/grl.50308.

——, N. Sakaeda, G. N. Kiladis, and K. Kikuchi, 2017: Influences of the MJO on space-time tropical convection organization. *J. Geophys. Res.*, in press.

Dorman, C. E., and R. H. Bourke, 1979: Precipitation over the Pacific Ocean, 30°S to 60°N. *Mon. Wea. Rev.*, **107**, 896–910, doi:10.1175/1520-0493(1979)107<0896:POTPOT>2.0.CO;2.

Feng, Z., S. Hagos, A. K. Rowe, C. D. Burleyson, M. N. Martini, and S. P. de Szoeke, 2015: Mechanisms of convective cloud organization by cold pools over tropical warm ocean during the AMIE/DYNAMO field campaign. *J. Adv. Model. Earth Syst.*, **7**, 357–381, doi:10.1002/2014MS000384.

Fujita, M., K. Yoneyama, S. Mori, T. Nasuno, and M. Satoh, 2011: Diurnal convection peaks over the eastern Indian Ocean off Sumatra during different MJO phases. J. Meteor. Soc. Japan, **89A**, 317–330, doi:10.2151/jmsj.2011-A22.

Gray, W. M., and R. W. Jacobson, 1977: Diurnal variation of deep cumulus convection. *Mon. Wea. Rev.*, **105**, 1171–1188, doi:10.1175/1520-0493(1977)105<1171:DVODCC>2.0.CO;2.

Hagos, S. M., C. Zhang, Z. Feng, C. D. Burleyson, C. DeMott, B. Kerns, J. J. Benedict, and M. N. Martini, 2016: The impact of the diurnal cycle on the propagation of Madden–Julian oscillation convection across the maritime continent. *J. Adv. Model. Earth Syst.*, **8**, 1552–1564, doi:10.1002/2016MS000725.

Hartmann, D. L., and E. E. Recker, 1986: Diurnal variation of outgoing longwave radiation in the tropics. *J. Climate Appl. Meteor.*, **25**, 800–812, doi:10.1175/1520-0450(1986)025<0800:DVOOLR>2.0.CO;2.

Hassim, M. E. E., T. P. Lane, and W. W. Grabowski, 2016: The diurnal cycle of rainfall over New Guinea in convection-permitting WRF simulations. *Atmos. Chem. Phys.*, **16**, 161–175, doi:10.5194/acp-16-161-2016.

Hendon, H. H., and K. Woodberry, 1993: The diurnal cycle of tropical convection. *J. Geophys. Res.*, **98**, 16 623–16 637, doi:10.1029/93JD00525.

——, and B. Liebmann, 1994: Organization of convection within the Madden–Julian oscillation. *J. Geophys. Res.*, **99**, 8073–8083, doi:10.1029/94JD00045.

Houze, R. A., S. G. Geotis, F. D. Marks Jr, and A. K. West, 1981: Winter monsoon convection in the vicinity of north Borneo. Part I: Structure and time variation of the clouds and precipitation. *Mon. Wea. Rev.*, **109**, 1595–1614, doi:10.1175/1520-0493(1981)109<1595:WMCITV>2.0.CO;2.

Huffman, G. J., and Coauthors, 2007: The TRMM Multisatellite Precipitation Analysis (TMPA): Quasi-global, multiyear,

combined-sensor precipitation estimates at fine scales. *J. Hydrometeor.*, **8**, 38–55, doi:10.1175/JHM560.1.

Ichikawa, H., and T. Yasunari, 2006: Time–space characteristics of diurnal rainfall over Borneo and surrounding oceans as observed by TRMM-PR. *J. Climate*, **19**, 1238–1260, doi:10.1175/JCLI3714.1.

——, and ——, 2008: Intraseasonal variability in diurnal rainfall over New Guinea and the surrounding oceans during austral summer. *J. Climate*, **21**, 2852–2868, doi:10.1175/2007JCLI1784.1.

Iguchi, T., T. Kozu, R. Meneghini, J. Awaka, and K. Okamoto, 2000: Rain-profiling algorithm for the TRMM Precipitation Radar. *J. Appl. Meteor.*, **39**, 2038–2052, doi:10.1175/1520-0450(2001)040<2038:RPAFTT>2.0.CO;2.

Janowiak, J. E., P. A. Arkin, and M. Morrissey, 1994: An examination of the diurnal cycle in oceanic tropical rainfall using satellite and in situ data. *Mon. Wea. Rev.*, **122**, 2296–2311, doi:10.1175/1520-0493(1994)122<2296:AEOTDC>2.0.CO;2.

Johnson, R. H., T. M. Rickenbach, S. A. Rutledge, P. E. Ciesielski, and W. H. Schubert, 1999: Trimodal characteristics of tropical convection. *J. Climate*, **12**, 2397–2418, doi:10.1175/1520-0442(1999)012<2397:TCOTC>2.0.CO;2.

Jones, C., L. M. V. Carvalho, R. W. Higgins, D. E. Waliser, and J.- K. E. Schemm, 2004: Climatology of tropical intraseasonal convective anomalies: 1979–2002. *J. Climate*, **17**, 523–539, doi:10.1175/1520-0442(2004)017<0523:COTICA>2.0.CO;2.

Kanamori, H., T. Yasunari, and K. Kuraji, 2013: Modulation of the diurnal cycle of rainfall associated with the MJO observed by a dense hourly rain gauge network at Sarawak, Borneo. *J. Climate*, **26**, 4858–4875, doi:10.1175/JCLI-D-12-00158.1.

Keenan, T. D., and R. E. Carbone, 2008: Propagation and diurnal evolution of warm season cloudiness in the Australian and Maritime Continent region. *Mon. Wea. Rev.*, **136**, 973–994, doi:10.1175/2007MWR2152.1.

Kerns, B. W., and S. S. Chen, 2016: Large-scale precipitation tracking and the MJO over the Maritime Continent and Indo-Pacific warm pool. *J. Geophys. Res. Atmos.*, **121**, 8755–8776, doi:10.1002/2015JD024661.

Kikuchi, K., and B. Wang, 2008: Diurnal precipitation regimes in the global tropics. *J. Climate*, **21**, 2680–2696, doi:10.1175/2007JCLI2051.1.

——, G. N. Kiladis, J. Dias, and T. Nasuno, 2017: Convectively coupled equatorial waves during CINDY/DYNAMO: Slow Kelvin waves as building blocks. *Climate Dyn.*, in press.

Kiladis, G. N., K. H. Straub, and P. T. Haertel, 2005: Zonal and vertical structure of the Madden–Julian Oscillation. *J. Atmos. Sci.*, **62**, 2790–2809, doi:10.1175/JAS3520.1.

——, J. Dias, K. H. Straub, M. C. Wheeler, S. N. Tulich, K. Kikuchi, K. M. Weickmann, and M. J. Ventrice, 2014: A comparison of OLR and circulation-based indices for tracking the MJO. *Mon. Wea. Rev.*, **142**, 1697–1715, doi:10.1175/MWR-D-13-00301.1.

——, ——, and M. Gehne, 2016: The relationship between equatorial mixed Rossby–gravity and eastward inertio-gravity waves. Part I. *J. Atmos. Sci.*, **73**, 2123–2145, doi:10.1175/JAS-D-15-0230.1.

Kousky, V. E., 1980: Diurnal rainfall variation in northeast Brazil. *Mon. Wea. Rev.*, **108**, 488–498, doi:10.1175/1520-0493(1980)108<0488:DRVINB>2.0.CO;2.

Kraus, E. B., 1963: The diurnal precipitation change over the sea. *J. Atmos. Sci.*, **20**, 551–556, doi:10.1175/1520-0469(1963)020<0551:TDPCOT>2.0.CO;2.

Kummerow, C., and Coauthors, 2001: The evolution of the Goddard profiling algorithm (GPROF) for rainfall estimation from passive microwave sensors. *J. Appl. Meteor.*, **40**, 1801–1820, doi:10.1175/1520-0450(2001)040<1801:TEOTGP>2.0.CO;2.

Liebmann, B., and C. A. Smith, 1996: Description of a complete (interpolated) outgoing longwave radiation dataset. *Bull. Amer. Meteor. Soc.*, **77**, 1275–1277.

Madden, R. A., and P. R. Julian, 1971: Detection of a 40–50 day oscillation in the zonal wind in the tropical Pacific. *J. Atmos. Sci.*, **28**, 702–708, doi:10.1175/1520-0469(1971)028<0702:DOADOI>2.0.CO;2.

——, and ——, 1972: Description of global-scale circulation cells in the tropics with a 40–50 day period. *J. Atmos. Sci.*, **29**, 1109–1123, doi:10.1175/1520-0469(1972)029<1109:DOGSCC>2.0.CO;2.

Majda, A. J., and S. N. Stechmann, 2009: The skeleton of tropical intraseasonal oscillations. *Proc. Natl. Acad. Sci. USA*, **106**, 8417–8422, doi:10.1073/pnas.0903367106.

——, and Q. Yang, 2016: A multiscale model for the intraseasonal impact of the diurnal cycle over the Maritime Continent on the Madden–Julian oscillation. *J. Atmos. Sci.*, **73**, 579–604, doi:10.1175/JAS-D-15-0158.1.

Maloney, E. D., 2009: The moist static energy budget of a composite tropical intraseasonal oscillation in a climate model. *J. Climate*, **22**, 711–729, doi:10.1175/2008JCLI2542.1.

Mapes, B. E., T. T. Warner, M. Xu, and A. J. Negri, 2003: Diurnal patterns of rainfall in northwestern South America. Part I: Observations and context. *Mon. Wea. Rev.*, **131**, 799–812, doi:10.1175/1520-0493(2003)131<0799:DPORIN>2.0.CO;2.

Matthews, A. J., G. Pickup, S. C. Peatman, P. Clews, and J. Martin, 2013: The effect of the Madden–Julian oscillation on station rainfall and river level in the Fly River system, Papua New Guinea. *J. Geophys. Res. Atmos.*, **118**, 10 926–10 935, doi:10.1002/jgrd.50865.

——, D. B. Baranowski, K. J. Heywood, P. J. Flatau, and S. Schmidtko, 2014: The surface diurnal warm layer in the Indian Ocean during CINDY/DYNAMO. *J. Climate*, **27**, 9101–9122, doi:10.1175/JCLI-D-14-00222.1.

Mori, S., and Coauthors, 2004: Diurnal land–sea rainfall peak migration over Sumatera Island, Indonesian Maritime Continent, observed by TRMM satellite and intensive rawinsonde soundings. *Mon. Wea. Rev.*, **132**, 2021–2039, doi:10.1175/1520-0493(2004)132<2021:DLRPMO>2.0.CO;2.

Myers, D. S., and D. E. Waliser, 2003: Three-dimensional water vapor and cloud variations associated with the Madden–Julian oscillation during Northern Hemisphere winter. *J. Climate*, **16**, 929–950, doi:10.1175/1520-0442(2003)016<0929:TDWVAC>2.0.CO;2.

Nakazawa, T., 1988: Tropical super clusters within intraseasonal variations over the western Pacific. *J. Meteor. Soc. Japan*, **66**, 823–839.

Neale, R., and J. Slingo, 2003: The Maritime Continent and its role in the global climate: A GCM study. *J. Climate*, **16**, 834–848, doi:10.1175/1520-0442(2003)016<0834:TMCAIR>2.0.CO;2.

Negri, A. J., T. L. Bell, and L. Xu, 2002: Sampling of the diurnal cycle of precipitation using TRMM. *J. Atmos. Oceanic Technol.*, **19**, 1333–1344, doi:10.1175/1520-0426(2002)019<1333:SOTDCO>2.0.CO;2.

Nesbitt, S. W., and E. J. Zipser, 2003: The diurnal cycle of rainfall and convective intensity according to three years of TRMM measurements. *J. Climate*, **16**, 1456–1475, doi:10.1175/1520-0442-16.10.1456.

Nitta, T., and S. Sekine, 1994: Diurnal variation of convective activity over the tropical western Pacific. *J. Meteor. Soc. Japan*, **72**, 627–641.

Oh, J.-H., K.-Y. Kim, and G.-H. Lim, 2012: Impact of MJO on the diurnal cycle of rainfall over the western Maritime Continent in the austral summer. *Climate Dyn.*, **38**, 1167–1180, doi:10.1007/s00382-011-1237-4.

Peatman, S. C., A. J. Matthews, and D. P. Stevens, 2014: Propagation of the Madden–Julian Oscillation through the Maritime Continent and scale interaction with the diurnal cycle of precipitation. *Quart. J. Roy. Meteor. Soc.*, **140**, 814–825, doi:10.1002/qj.2161.

——, ——, and ——, 2015: Propagation of the Madden–Julian Oscillation and scale interaction with the diurnal cycle in a high-resolution GCM. *Climate Dyn.*, **45**, 2901–2918, doi:10.1007/s00382-015-2513-5.

Powell, S. W., and R. A. Houze, 2015: Evolution of precipitation and convective echo top heights observed by TRMM radar over the Indian Ocean during DYNAMO. *J. Geophys. Res. Atmos.*, **120**, 3906–3919, doi:10.1002/2014JD022934.

Randall, D. A., Harshvardhan, and D. A. Dazlich, 1991: Diurnal variability of the hydrologic cycle in a general circulation model. *J. Atmos. Sci.*, **48**, 40–62, doi:10.1175/1520-0469(1991)048<0040:DVOTHC>2.0.CO;2.

Rauniyar, S. P., and K. J. E. Walsh, 2011: Scale interaction of the diurnal cycle of rainfall over the Maritime Continent and Australia: Influence of the MJO. *J. Climate*, **24**, 325–348, doi:10.1175/2010JCLI3673.1.

Raupp, C. F. M., and P. L. Silva Dias, 2009: Resonant wave interactions in the presence of a diurnally varying heat source. *J. Atmos. Sci.*, **66**, 3165–3183, doi:10.1175/2009JAS2899.1.

Romilly, T. G., and M. Gebremichael, 2011: Evaluation of satellite rainfall estimates over Ethiopian river basins. *Hydrol. Earth Syst. Sci.*, **15**, 1505–1514, doi:10.5194/hess-15-1505-2011.

Rossow, W. B., and R. A. Schiffer, 1999: Advances in understanding clouds from ISCCP. *Bull. Amer. Meteor. Soc.*, **80**, 2261–2287, doi:10.1175/1520-0477(1999)080<2261:AIUCFI>2.0.CO;2.

Roundy, P. E., and W. M. Frank, 2004: A climatology of waves in the equatorial region. *J. Atmos. Sci.*, **61**, 2105–2132, doi:10.1175/1520-0469(2004)061<2105:ACOWIT>2.0.CO;2.

Rowe, A. K., and R. A. Houze, 2015: Cloud organization and growth during the transition from suppressed to active MJO conditions. *J. Geophys. Res. Atmos.*, **120**, 10 324–10 350, doi:10.1002/2014JD022948.

Ruppert, J. H., and R. H. Johnson, 2015: Diurnally modulated cumulus moistening in the preonset stage of the Madden–Julian oscillation during DYNAMO. *J. Atmos. Sci.*, **72**, 1622–1647, doi:10.1175/JAS-D-14-0218.1.

——, and ——, 2016: On the cumulus diurnal cycle over the tropical warm pool. *J. Adv. Model. Earth Syst.*, **8**, 669–690, doi:10.1002/2015MS000610.

Sakurai, N., and Coauthors, 2005: Diurnal cycle of cloud system migration over Sumatera Island. *J. Meteor. Soc. Japan*, **83**, 835–850, 10.2151/jmsj.83.835.

Slingo, J., P. Inness, R. Neale, S. Woolnough, and G. Yang, 2003: Scale interactions on diurnal to seasonal timescales and their relevance to model systematic errors. *Ann. Geophys.*, **46**, 139–155, doi:10.4401/ag-3383.

Straub, K. H., 2013: MJO initiation in the real-time multivariate MJO index. *J. Climate*, **26**, 1130–1151, doi:10.1175/JCLI-D-12-00074.1.

——, and G. N. Kiladis, 2003: Interactions between the boreal summer intraseasonal oscillation and higher-frequency tropical wave activity. *Mon. Wea. Rev.*, **131**, 945–960, doi:10.1175/1520-0493(2003)131<0945:IBTBSI>2.0.CO;2.

Sui, C.-H., and K.-M. Lau, 1992: Multiscale phenomena in the tropical atmosphere over the western Pacific. *Mon. Wea. Rev.*, **120**, 407–430, doi:10.1175/1520-0493(1992)120<0407:MPITTA>2.0.CO;2.

——, ——, Y. N. Takayabu, and D. A. Short, 1997: Diurnal variations in tropical oceanic cumulus convection during TOGA COARE. *J. Atmos. Sci.*, **54**, 639–655, doi:10.1175/1520-0469(1997)054<0639:DVITOC>2.0.CO;2.

Suzuki, T., 2009: Diurnal cycle of deep convection in super clusters embedded in the Madden–Julian oscillation. *J. Geophys. Res.*, **114**, D22102, doi:10.1029/2008JD011303.

Tabata, Y., H. Hashiguchia, M. K. Yamamoto, M. Yamamoto, M. D. Yamanaka, S. Mori, F. Syamsudinc, and T. Manik, 2011: Observational study on diurnal precipitation cycle in equatorial Indonesia using 1.3-GHz wind profiling radar network and TRMM Precipitation Radar. *J. Atmos. Sol. Terr. Phys.*, **73**, 1031–1042, doi:10.1016/j.jastp.2010.10.003.

Tian, B., D. E. Waliser, and E. J. Fetzer, 2006: Modulation of the diurnal cycle of tropical deep convective clouds by the MJO. *Geophys. Res. Lett.*, **33**, L20704, doi:10.1029/2006GL027752.

Tulich, S. N., and G. N. Kiladis, 2012: Squall lines and convectively coupled gravity waves in the tropics: Why do most cloud systems propagate westward? *J. Atmos. Sci.*, **69**, 2995–3012, doi:10.1175/JAS-D-11-0297.1.

Vincent, C. L., T. P. Lane, and M. C. Wheeler, 2016: A local index of Maritime Continent intraseasonal variability based on rain rates over the land and sea. *Geophys. Res. Lett.*, **43**, 9306–9314, doi:10.1002/2016GL069987.

Wheeler, M., and G. Kiladis, 1999: Convectively coupled equatorial waves: Analysis of clouds in the wavenumber–frequency domain. *J. Atmos. Sci.*, **56**, 374–399, doi:10.1175/1520-0469(1999)056<0374:CCEWAO>2.0.CO;2.

——, and H. H. Hendon, 2004: An all-season real-time multivariate MJO index: Development of an index for monitoring and prediction. *Mon. Wea. Rev.*, **132**, 1917–1932, doi:10.1175/1520-0493(2004)132<1917:AARMMI>2.0.CO;2.

Xu, W., and S. A. Rutledge, 2014: Convective characteristics of the Madden–Julian oscillation over the central Indian Ocean observed by shipborne radar during DYNAMO. *J. Atmos. Sci.*, **71**, 2859–2877, doi:10.1175/JAS-D-13-0372.1.

Yamamoto, M. K., F. A. Furuzawa, A. Higuchi, and K. Nakamura, 2008: Comparison of diurnal variations in precipitation systems observed by TRMM PR, TMI, and VIRS. *J. Climate*, **21**, 4011–4028, doi:10.1175/2007JCLI2079.1.

Yang, D., and A. P. Ingersoll, 2011: Testing the hypothesis that the MJO is a mixed Rossby–gravity wave packet. *J. Atmos. Sci.*, **68**, 226–239, doi:10.1175/2010JAS3563.1.

——, and ——, 2013: Triggered convection, gravity waves, and the MJO: A shallow-water model. *J. Atmos. Sci.*, **70**, 2476–2486, doi:10.1175/JAS-D-12-0255.1.

Yang, G.-Y., and J. Slingo, 2001: The diurnal cycle in the tropics. *Mon. Wea. Rev.*, **129**, 784–801, doi:10.1175/1520-0493(2001)129<0784:TDCITT>2.0.CO;2.

Yang, S., and E. A. Smith, 2006: Mechanisms for diurnal variability of global tropical rainfall observed from TRMM. *J. Climate*, **19**, 5190–5226, doi:10.1175/JCLI3883.1.

——, and ——, 2008: Convective–stratiform precipitation variability at seasonal scale from 8 yr of TRMM observations: Implications for multiple modes of diurnal variability. *J. Climate*, **21**, 4087–4114, doi:10.1175/2008JCLI2096.1.

Yasunaga, K., and B. Mapes, 2012: Differences between more divergent and more rotational types of convectively coupled equatorial waves. Part I: Space–time spectral analyses. *J. Atmos. Sci.*, **69**, 3–16, doi:10.1175/JAS-D-11-033.1.

Zhang, C., and M. Dong, 2004: Seasonality in the Madden–Julian oscillation. *J. Climate*, **17**, 3169–3180, doi:10.1175/1520-0442(2004)017<3169:SITMO>2.0.CO;2.

Zuluaga, M. D., and R. A. Houze, 2013: Evolution of the population of precipitating convective systems over the equatorial Indian Ocean in active phases of the Madden–Julian Oscillation. *J. Atmos. Sci.*, **70**, 2713–2725, doi:10.1175/JAS-D-12-0311.1.